The EDS1–PAD4–ADR1 node mediates *Arabidopsis* pattern-triggered immunity

Rory N. Pruitt[1,13], Federica Locci[2,13], Friederike Wanke[3], Lisha Zhang[1], Svenja C. Saile[3], Anna Joe[1], Darya Karelina[4], Chenlei Hua[1], Katja Fröhlich[1], Wei-Lin Wan[1,11], Meijuan Hu[5], Shaofei Rao[5,12], Sara C. Stolze[6], Anne Harzen[6], Andrea A. Gust[1], Klaus Harter[3], Matthieu H. A. J. Joosten[7], Bart P. H. J. Thomma[7,8], Jian-Min Zhou[5], Jeffery L. Dangl[9], Detlef Weigel[4], Hirofumi Nakagami[6], Claudia Oecking[3], Farid El Kasmi[3], Jane E. Parker[2,8 ✉] & Thorsten Nürnberger[1,10 ✉]

Plants deploy cell-surface and intracellular leucine rich-repeat domain (LRR) immune receptors to detect pathogens[1]. LRR receptor kinases and LRR receptor proteins at the plasma membrane recognize microorganism-derived molecules to elicit pattern-triggered immunity (PTI), whereas nucleotide-binding LRR proteins detect microbial effectors inside cells to confer effector-triggered immunity (ETI). Although PTI and ETI are initiated in different host cell compartments, they rely on the transcriptional activation of similar sets of genes[2], suggesting pathway convergence upstream of nuclear events. Here we report that PTI triggered by the *Arabidopsis* LRR receptor protein RLP23 requires signalling-competent dimers of the lipase-like proteins EDS1 and PAD4, and of ADR1 family helper nucleotide-binding LRRs, which are all components of ETI. The cell-surface LRR receptor kinase SOBIR1 links RLP23 with EDS1, PAD4 and ADR1 proteins, suggesting the formation of supramolecular complexes containing PTI receptors and transducers at the inner side of the plasma membrane. We detected similar evolutionary patterns in LRR receptor protein and nucleotide-binding LRR genes across *Arabidopsis* accessions; overall higher levels of variation in LRR receptor proteins than in LRR receptor kinases are consistent with distinct roles of these two receptor families in plant immunity. We propose that the EDS1–PAD4–ADR1 node is a convergence point for defence signalling cascades, activated by both surface-resident and intracellular LRR receptors, in conferring pathogen immunity.

Arabidopsis thaliana (hereafter *Arabidopsis*) cell-surface LRR receptor kinases (LRR-RKs) and LRR receptor protein (LRR-RP)–SOBIR1 complexes recruit the co-receptor BAK1 and signal through receptor-like cytoplasmic kinases (RLCKs) to elicit PTI[3]. Intracellular coiled-coil (CC)-nucleotide-binding LRR (NLR) or TOLL-INTERLEUKIN 1 RECEPTOR (TIR)-NLR receptors[4] require ADR1-type and NRG1-type helper NLRs (hNLRs) and the lipase-like EDS1 family proteins EDS1, PAD4 and SAG101 to confer ETI[5,6]. While the defence outputs for PTI and ETI are qualitatively similar[2], where and how pathways activated in different cell compartments converge remain unclear. Effective plant defence relies on mutual potentiation of PTI and ETI pathways[7,8], suggesting mechanistic links between these two tiers of the plant immune system.

RLCKs PBL30 and PBL31 mediate PTI

The *Arabidopsis* class VII RLCK (RLCK-VII) BIK1 promotes LRR-RK-mediated PTI but is a negative regulator of LRR-RP-mediated PTI[9]. To identify RLCK-VII members with positive roles in LRR-RP-dependent PTI, we screened an *Arabidopsis* RLCK-VII transfer DNA mutant library[10] for ethylene production elicited by fungal pg13(At)[11], oomycete nlp20 and bacterial eMax (which are recognized by RLP42, RLP23 and RLP1, respectively)[3] (Extended Data Fig. 1a). A *pbl31* mutant was defective in response to these elicitors compared with wild-type plants (Columbia-0 (Col-0)) (Extended Data Fig. 1a). PBL31 belongs to RLCK-VII subfamily 7, together with PBL30 (also known as CST) and PBL32 (ref. [10]). The LRR-RP elicitors nlp20, eMax
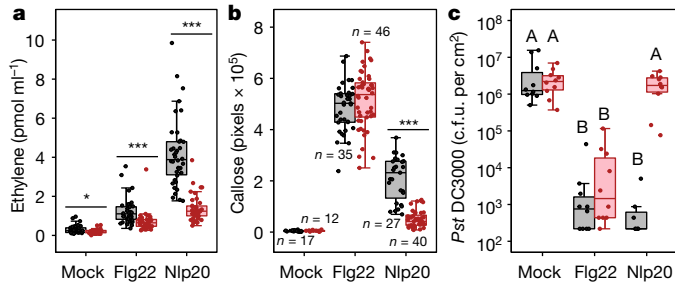
Fig. 1 | RLCK-VII-7 subfamily members are required for LRR-RP-mediated immunity. a, Elicitor-induced ethylene production in Col-0 and the *pbl30 pbl31 pbl32* mutant (grey and pink, respectively, in all panels). *n* = 38 (nlp20) or 36 (mock and flg22) samples, each comprising 3 leaf pieces. Data are from 10 independent experiments. For **a**, **b**, a two-sided Wilcoxon rank-sum test with continuity correction was used to analyse significant differences between Col-0 and the *pbl30 pbl31 pbl32* mutant for the given elicitor treatment (*$P \leq 0.05$, ***$P \leq 0.0001$). **b**, Callose deposition in Col-0 and the *pbl30 pbl31 pbl32* mutant. *n* ≥ 12 images from at least 3 leaves; exact *n* values are provided in the graph. **c**, Elicitor-induced defence against infection is impaired in the *pbl30 pbl31 pbl32* mutant. Leaves were infiltrated with the indicated elicitor and challenged with *Pst* DC3000 after 24 h. Boxes show bacterial colonization 3 d after infection. *n* = 10 (for Col-0) and *n* = 7 (for nlp20) biological replicates, each comprising 2 leaf discs. Data points with different letters indicate significant differences of $P \leq 0.05$ (Kruskal–Wallis test with a post-hoc two-sided Steel–Dwass test). c.f.u., colony forming units. For the box plots, the centre line indicates the median, the bounds of the box show the 25th and the 75th percentiles, and the whiskers indicate 1.5 × IQR (that is, the interquartile range between the 25th and the 75th percentile). Experiments in **b** and **c** were performed at least three times with similar results. Exact *P* values for all experiments are provided in Supplementary Table 5.

and IF1 (which is recognized by RLP32)[12] triggered a reduced ethylene response in a *pbl30* mutant, although in some cases, differences were not statistically significant; responses in the *pbl32* mutant were not impaired to any elicitor (Extended Data Fig. 1). Ethylene production in *pbl30 pbl31* double mutant and *pbl30 pbl31 pbl32* triple mutant lines was reduced more strongly than in any single mutant (Extended Data Fig. 1b). The LRR-RK elicitors flg22 and elf18, which activate the LRR-RKs FLS2 and EFR[3], respectively, also induced lower ethylene responses in *pbl30 pbl31* and *pbl30 pbl31 pbl32* mutants than in the wild type, but to a lesser extent than observed for LRR-RP elicitors (Fig. 1a, Extended Data Fig. 1b). Nlp20-induced ethylene production in *pbl30 pbl31 pbl32* mutants was complemented by overexpression of PBL31, but not by the kinase-inactive variant PBL31[K201A] (Extended Data Fig. 2a–c).

We tested whether the RLCK-VII-7 subfamily mediates other RLP23-mediated immunity outputs. Nlp20-induced production of reactive oxygen species (ROS) was virtually abolished in *pbl30 pbl31* and *pbl30 pbl31 pbl32* mutants, whereas flg22-induced ROS production was reduced (Extended Data Fig. 3a, b). Nlp20-triggered callose deposition was strongly impaired in *pbl30 pbl31* and *pbl30 pbl31 pbl32* mutants, whereas flg22-triggered callose production was unaltered in these mutants (Fig. 1b, Extended Data Fig. 3c). Nlp20-induced expression of the phytoalexin synthesis genes *PAD3* and *CYP71A13* (ref. [13]) and the systemic acquired resistance marker *FMO1* (ref. [14]) was impaired in *pbl30 pbl31 pbl32* leaves (Extended Data Fig. 3d). Inhibition of seedling growth in the presence of elf18 or flg22 (a response unaffected by LRR-RP ligands[15]) was similar in Col-0 and the *pbl30 pbl31 pbl32* mutant, and both lines displayed similar levels of nlp20-induced and flg22-induced MAPK phosphorylation (Extended Data Fig. 3e, f). These results identify the roles of the RLCK-VII-7 family RLCKs PBL30 and PBL31 in a subset of PTI responses.

We found that nlp20–RLP23-induced resistance to infection by virulent *Pseudomonas syringae* pv. *tomato* (*Pst*) DC3000 was abolished in

pbl30 pbl31 and *pbl30 pbl31 pbl32* mutants, whereas flg22-induced resistance was reduced (Fig. 1c, Extended Data Fig. 3g). ETI conferred by the TIR-NLR receptor pair RRS1–RPS4 or the CC-NLR RPS2 was unaffected in the *pbl30 pbl31 pbl32* mutant (Extended Data Fig. 3h). Hence, PBL30 and PBL31 are dispensable for ETI but are essential positive regulators of LRR-RP-mediated PTI, with less prominent roles in LRR-RK-mediated PTI.

EDS1–PAD4 dimers mediate PTI

EDS1 forms exclusive heterodimers with SAG101 or PAD4 that control different immunity branches in ETI[5,16,17]. *Arabidopsis* EDS1–PAD4 dimers promote not only ETI transcriptional defence but also basal immunity[18,19]. Accordingly, *eds1* and *pad4* mutants are hypersusceptible to pathogens without recognized effectors[5]. To test whether reduced basal immunity is due to impaired PTI signalling, we measured PTI responses in *pad4*, *eds1* and *sag101* mutants (Fig. 2, Extended Data Fig. 4). *Pad4* and *eds1*, but not *sag101*, mutants produced substantially less ethylene than the wild type in response to nlp20, IF1 and pg13(At) (Fig. 2a, Extended Data Fig. 4a). Ethylene production mediated by FLS2 and EFR was not significantly reduced in *pad4* and *eds1* mutants (Fig. 2a, Extended Data Fig. 4a).

An EDS1 variant (EDS1[LLIF]) that cannot dimerize with PAD4 (ref. [19]) failed to restore LRR-RP-mediated ethylene responses (Fig. 2b, Extended Data Fig. 4a). Likewise, mutation of a cationic residue (EDS1[R493A]) at a signalling surface in the EDS1–PAD4 dimer that disables ETI[20] also abolished RLP23-mediated ethylene production (Fig. 2b). EDS1 and PAD4 variants (EDS1[SDH] and PAD4[S]) with mutations in their putative α/β-hydrolase catalytic residues are functional in ETI and basal immunity[19] and also fully complement nlp20-induced ethylene production in an *eds1 pad4* mutant (Extended Data Fig. 4b). Fungal thaxtomin A, a selective activator of PAD4-dependent immunity[21], enhanced nlp20-induced, but not flg22-induced, ethylene production in Col-0 but not in the *pad4* mutant (Extended Data Fig. 4c). These data indicate predominant involvement of the EDS1–PAD4 dimer in LRR-RP signalling.

The production of ROS and callose was strongly reduced in *pad4* and *eds1* mutants upon nlp20, but not flg22, treatment (Fig. 2c, d). Moreover, nlp20-triggered *PAD3*, *CYP71A13* and *FMO1* transcript accumulation was reduced in the *pad4* mutant compared with wild-type Col-0 (Extended Data Fig. 4d). Inhibition of seedling growth in the presence of flg22 or elf18 was similar in Col-0 and the *pad4* mutant (Extended Data Fig. 4e), as was elicitor-induced MAPK activation (Extended Data Fig. 4f). In induced pathogen resistance assays, nlp20 failed to confer protection to *Pst* DC3000 infection in *pad4* and *eds1* mutants; flg22-induced resistance was also partially impaired in these mutants (Fig. 2e). Both elicitors conferred full protection in the *sag101* mutant (Fig. 2e). We concluded that a signalling-competent EDS1–PAD4 complex is essential for many aspects of NLR-mediated ETI, for LRR-RP-mediated PTI and partly for LRR-RK signalling.

To assess possible regulatory effects of PAD4 on the expression of PTI-associated genes, we measured transcript levels of key receptor, co-receptor and signalling components in *pad4* and Col-0 plants. All transcript levels were similar in both genotypes (Extended Data Fig. 5a), and transcriptomic data suggest similar transcript levels in *eds1* and *adr1* triple genotypes[20,22]. Likewise, accumulation of BAK1, FLS2, MPK3, MPK4 and MPK6 proteins was similar between Col-0 and the *pad4* mutant (Extended Data Fig. 5b). These data, together with intact elicitor-induced MAPK activation in the *eds1 pad4 sag101* mutant (Extended Data Fig. 4f), suggest that machineries involved in early PTI signalling are not severely affected by the lack of EDS1 and PAD4.

ADR1 family hNLRs signal in PTI

Arabidopsis EDS1–SAG101 dimers work with NRG1 family hNLRs in TIR-NLR ETI signalling[16,17]. By contrast, EDS1–PAD4 dimers function
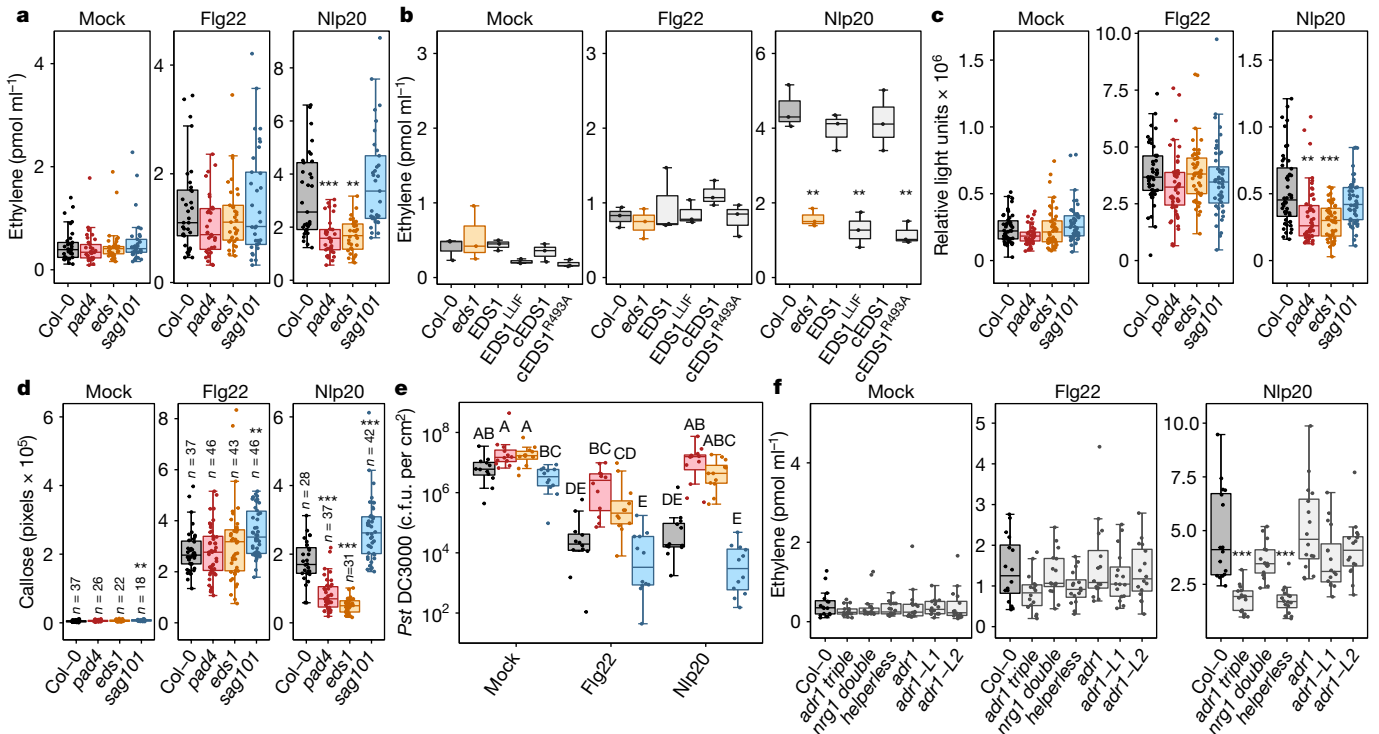
Fig. 2 | PAD4, EDS1 and ADR1 helper NLRs are positive regulators of LRR-RP signalling. a, Elicitor-induced ethylene production in Col-0, *pad4*, *eds1* and *sag101* mutants (grey, pink, orange and blue, respectively, in all panels). *n* = 33, each from 3 leaf pieces. Data are from eight independent experiments. For **a**, **c**, **d** and **f**, statistical differences between Col-0 and the indicated mutants were analysed using a Kruskal–Wallis test with a post-hoc two-sided Steel–Dwass test (**P ≤ 0.01, ***P ≤ 0.0001). **b**, Ethylene production depends on the PAD4–EDS1 heterodimer. *n* = 3, each from 3 leaf pieces. Statistical differences between Col-0 and the indicated mutants were analysed by two-sided Welch's pairwise tests (**P ≤ 0.01). For the complementation constructs cEDS1 and EDS1, see Supplementary Table 3. **c**, Total elicitor-induced ROS production over 30 min. *n* = 48 leaf pieces from 3 independent experiments. **d**, Callose deposition in Col-0, *pad4*, *eds1* and *sag101* mutants. *n* ≥ 12 images from at least

3 leaves; exact *n* values are indicated in the graph. **e**, Elicitor-induced defence against infection is impaired in *pad4* and *eds1* mutants. Leaves were infiltrated with the indicated elicitor and challenged with *Pst* DC3000 after 24 h. Boxes show bacterial colonization 3 d after infection. *n* = 12 biological replicates comprising 2 leaf discs. Data points with different letters indicate significant differences of *P* ≤ 0.05 (Kruskal–Wallis test with post-hoc two-sided Steel–Dwass test). **f**, Nlp20-induced ethylene production is dependent on ADR1 helper NLRs. *n* = 20, each from 3 leaf pieces. Data are from four independent experiments. For the box plots, the centre line indicates the median, the bounds of the box show the 25th and the 75th percentiles, and the whiskers indicate 1.5 × IQR. Experiments in **b**, **d** and **e** were performed at least three times with similar results. Exact *P* values for all experiments are provided in Supplementary Table 5.

with ADR1 family hNLRs to promote TIR-NLR ETI, CC-NLR ETI and basal immunity[16,17]. Consistent with our observations that LRR-RP responses require PAD4 but not SAG101, we found that nlp20 responses were strongly impaired in an *ADR1* family triple mutant (*adr1* triple)[22] but not an *NRG1* family double mutant (*nrg1* double)[22] (Fig. 2f, Extended Data Fig. 6a–c). A '*helperless*' mutant[22] lacking all *ADR1* and two functional full-length *NRG1* genes behaved similarly to the *adr1* triple mutant (Fig. 2f, Extended Data Fig. 6a–c). The *helperless* mutant was not impaired in elicitor-induced MAPK activation (Extended Data Fig. 6d) and was similar to Col-0 in seedling growth inhibition assays with flg22 or elf18 (Extended Data Fig. 6e). However, both nlp20-induced and flg22-induced resistance to *Pst* DC3000 was impaired in the *adr1* triple and *helperless* mutants compared with Col-0 (Extended Data Fig. 6f). Our data highlight a shared requirement of cell-surface-initiated PTI and intracellular ETI signalling for the EDS1–PAD4–ADR1 node.

SOBIR1 connects RLP23 to PAD4–EDS1–ADR1

Because PBL31 kinase, EDS1–PAD4 dimers and ADR1 family hNLRs have roles in LRR-RP-mediated PTI, including early responses such as ROS burst (Fig. 2c, Extended Data Figs. 3a, b, 6b), we tested for possible spatial proximity between RLP23 and the constitutively associated co-receptor SOBIR1 with these components by co-immunoprecipitation assays in *Nicotiana benthamiana* plants. Epitope-tagged RLP23 and

SOBIR1 precipitated PBL31 independent of nlp20 elicitation, suggesting a ligand-independent stable interaction between PBL31 and the receptor complex (Extended Data Fig. 7a). PBL31 was not precipitated by the GFP-tagged plasma membrane protein LTI6b (Extended Data Fig. 7a). Similarly, SOBIR1 interacted in a ligand-independent manner with PAD4, EDS1, ADR1 and the ADR1 isoforms ADR1-L1 and ADR1-L2 (Extended Data Fig. 7a, b). Bimolecular fluorescence complementation assays confirmed association between SOBIR1 and ADR1-L1 and ADR1-L2, but not ADR1, at the plasma membrane (Extended Data Fig. 7c, d). Spatial proximity of SOBIR1 with ADR1-L1, but not with PAD4 or EDS1, was corroborated in luciferase complementation assays (Extended Data Fig. 7e, f).

To investigate potential associations at the plasma membrane, we used fluorescently tagged proteins and assessed their spatial proximity by Förster resonance energy transfer by fluorescence lifetime (FLT) imaging (FRET-FLIM). Tested proteins (SOBIR1, ADR1, ADR1-L1, ADR1-L2, EDS1, PAD4, SAG101 and PBL31) localized, at least partly, to the plasma membrane when expressed in *N. benthamiana* (Extended Data Fig. 8a, b). Using SOBIR1–GFP as donor, we observed reduced GFP FLT in the presence of RFP-tagged EDS1, PAD4, PBL31, ADR1 and the ADR1 isoforms ADR1-L1 and ADR1-L2 (Fig. 3a). Because EDS1–PAD4 dimers mediate the RLP23 immune response (Fig. 2b), we co-expressed non-fluorescently labelled EDS1 with PAD4–RFP and vice versa with SOBIR1–GFP (Fig. 3a). Reduction in FLT was observed but was less pronounced than with
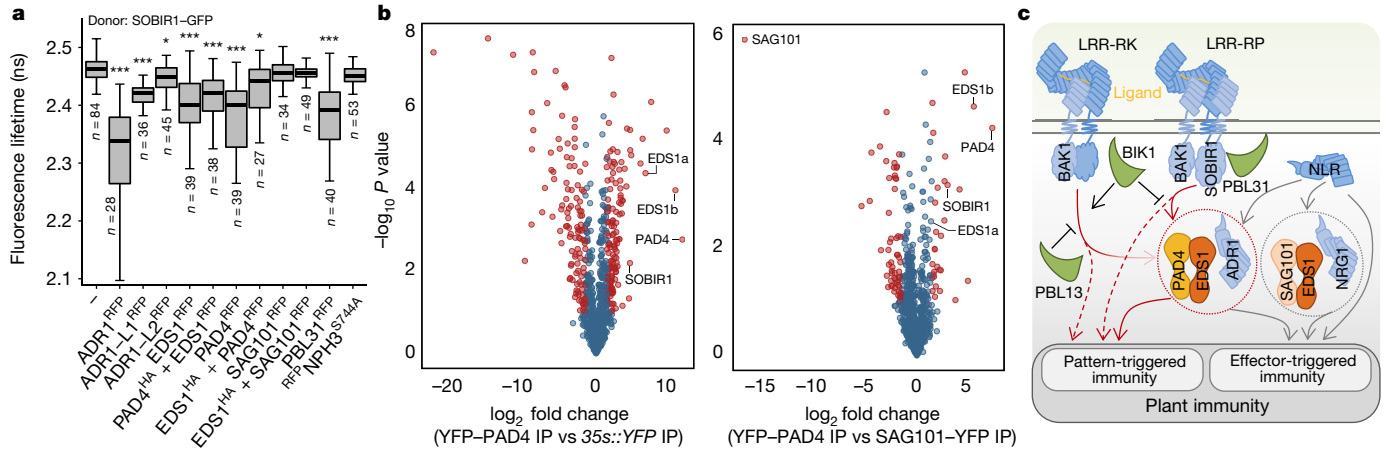
Fig. 3 | SOBIR1 associates with EDS1, PAD4 and ADR1 hNLRs to form a potential signalling node. a, FRET–FLIM reveals spatial proximity of SOBIR1 with PBL31, PAD4, EDS1 and ADR1 hNLRs. Membrane-associated NPH3^{S744A} serves as the control. Statistical differences in FLT between SOBIR1–GFP alone and the indicated FRET pair were analysed using a Kruskal–Wallis test with a post-hoc two-sided Steel–Dwass test (*$P \le 0.05$, ***$P \le 0.0001$). Exact P values are provided in Supplementary Table 5. $n \ge 27$ from at least 3 biological replicates. n values are shown below the boxes. The centre line indicates the median, the bounds of the box show the 25th and the 75th percentiles, and the whiskers indicate $1.5 \times$ IQR. ns, nanoseconds. **b**, SOBIR1 specifically co-purifies with YFP–PAD4 in *Arabidopsis* leaves. A *pad4 sag101* mutant complemented with YFP–PAD4 or SAG101–YFP, and wild-type Col-0 expressing *35S::YFP* (YFP), were used for IP assays. Volcano plots show normalized abundances of proteins detected by MS after IP of total protein extracts from 4.5-week-old leaves infiltrated with DMSO for 10 min. Corresponding data for nlp20-treated leaves

are provided in Extended Data Fig. 9a. The red dots indicate enriched proteins ($|\log_2(\text{YFP–PAD4/YFP})| \ge 1$ or $|\log_2(\text{YFP–PAD4/SAG101–YFP})| \ge 1$ using a permutation-based false discovery rate of 0.05). The two functional Col-0 EDS1 isoforms (EDS1a and EDS1b) were enriched in YFP–PAD4 samples, and EDS1a was enriched in SAG101–YFP IPs, as found in ETI-triggered tissues[16]. Samples were collected in four independent experiments. **c**, The EDS1–PAD4–ADR1 node mediates both PTI and ETI. Upon ligand perception, LRR-RK and LRR-RP receptors dimerize with BAK1 to activate PTI. The EDS1–PAD4–ADR1 node has a key role in LRR-RP signalling (red arrows) and a less prominent role in LRR-RK signalling (faded arrow). Some PTI outputs do not require EDS1–PAD4–ADR1 (dashed lines). ETI mediated by NLRs is dependent on the EDS1–PAD4–ADR1 and/or SAG101–EDS1–NRG1 nodes or is independent of either signalling node (grey arrows). The RLCK-VII kinases BIK1, PBL31 and PBL13 regulate LRR-RP and LRR-RK signalling.

SOBIR1–GFP and EDS1–RFP or PAD4–RFP alone (Fig. 3a). Reduction in FLT was not observed when SOBIR1–GFP was co-expressed with SAG101–RFP or plasma membrane-associated RFP–NPH3^{S744A} (ref. [23]) (Fig. 3a). While *Arabidopsis* SAG101 localizes primarily to nuclei[5,17], a small pool was detected close to the plasma membrane in these assays (Extended Data Fig. 8a, b). Using PBL31–GFP as donor confirmed its association with SOBIR1, ADR1-L1–RFP and EDS1–RFP, but not with ADR1–RFP, ADR1-L2–RFP, PAD4–RFP, SAG101–RFP or RFP–NPH3^{S744A} (Extended Data Fig. 8c). Co-expression of EDS1–haemagglutinin (HA) also led to reduction in FLT with the FRET pair PBL31–GFP + PAD4–RFP (Extended Data Fig. 8c), suggesting a close proximity of these proteins.

To monitor protein associations in *Arabidopsis*, we performed immunoprecipitations followed by tandem mass spectrometry (IP MS/MS) using *pad4 sag101* mutant lines stably expressing YFP–PAD4 or SAG101–YFP under control of their native promoters, and a wild-type Col-0 line constitutively expressing *p35S::YFP* as control[16]. Whereas RLCKs and ADR1 family members were not detected (Supplementary Tables 1, 2), SOBIR1 was enriched with YFP–PAD4 but not SAG101–YFP or YFP alone in mock-treated and nlp20-treated tissues and at 10 min or 3 h (Fig. 3b, Extended Data Fig. 9a–e). Together, the protein interaction data suggest that plasma membrane-resident LRR-RP–SOBIR1 receptors form a constitutive complex with PBL31 and components of the EDS1–PAD4–ADR1 node for PTI signalling.

LRR-RP and NLR genes are polymorphic

Having established that LRR-RPs and NLR immune receptors share signalling components, we assessed whether they have similar evolutionary patterns. Within species and populations, NLR genes have diversified, with signatures of both rapid and balancing evolution[24]. *Arabidopsis* LRR-RP-type immune receptors recognize widespread microbial surface patterns[3], but the encoding genes, like NLRs, often

occur within gene clusters[25]. To gauge LRR-RP gene variation, reads from 80 *Arabidopsis* accessions[26,27] were mapped onto the Col-0 reference genome. Genes were categorized as conserved, displaying complex variation, or exhibiting presence or absence polymorphisms. This within-species analysis revealed a similar proportion of variable genes in NLR and LRR-RP families, whereas LRR-RK genes had low variation, comparable to the genomic background (Extended Data Fig. 10a). LRR-RP genes encoding known receptors were found in all three classes: RLP23, RLP30 and RLP32 are conserved, RLP42 has a complex pattern, and RLP1 has a presence or absence polymorphism (Extended Data Fig. 10b). We conclude that LRR-RP and NLR genes have similar evolutionary dynamics in maintaining sequence diversity, whereas LRR-RK-encoding genes are more constrained.

Discussion

Cell-surface LRR-type receptors share a dependence on the EDS1–PAD4–ADR1 node with cytoplasmic NLRs for activating plant immunity (Fig. 3c). These signalling components are essential for LRR-RP-mediated immunity, whereas LRR-RK-induced defences rely partially on them (Fig. 2, Extended Data Figs. 4, 6). This finding, together with differential involvement of RLCKs in LRR-RP-mediated (PBL31 and BIK1) and LRR-RK-mediated (BIK1 and PBL13) PTI[9,28] (Fig. 1, Extended Data Figs. 1–3), supports the concept of distinct immune pathways being activated through different receptor systems[9] (Fig. 3c). A requirement for EDS1–PAD4–ADR1 in cell-surface and intracellular receptor-mediated immunity might explain similar defences upon activation of ETI or PTI[2].

We show that EDS1, PAD4, ADR1-type hNLRs and RLCK PBL31 reside in close proximity with transmembrane LRR-RP–SOBIR1 complexes in resting and elicited states (Fig. 3a, b, Extended Data Figs. 7–9). Thus, ligand-induced recruitment of the co-receptor BAK1 into

transmembrane complexes with LRR-RP-type receptors might initiate PTI signalling through a preformed SOBIR1-anchored platform at the plasma membrane.

Cell-surface LRR-RPs and cytoplasmic NLRs emerge as two polymorphic immune sensor classes (Extended Data Fig. 10). In contrast to NLRs, the LRR-RP repertoire includes conserved sensors for widespread microbial patterns[3,29], accession-specific polymorphic sensors for common patterns[11] and sequence-divergent sensors for microbial pathovar-specific effectors[29]. LRR-RPs confer partial (for example, RLP23)[3] or full (for example, Cf proteins)[29] resistance to host-adapted microbial pathovars. LRR-RPs thus qualify as sensors that mediate both PTI and ETI, which erodes the strict distinction between the two layers of innate immunity[29,30].

Online content

Any methods, additional references, Nature Research reporting summaries, source data, extended data, supplementary information, acknowledgements, peer review information; details of author contributions and competing interests; and statements of data and code availability are available at https://doi.org/10.1038/s41586-021-03829-0.

1. Jones, J. D. & Dangl, J. L. The plant immune system. *Nature* **444**, 323–329 (2006).
2. Lu, Y. & Tsuda, K. Intimate association of PRR- and NLR-mediated signaling in plant immunity. *Mol. Plant Microbe Interact.* **34**, 3–14 (2021).
3. Wan, W. L., Fröhlich, K., Pruitt, R. N., Nürnberger, T. & Zhang, L. Plant cell surface immune receptor complex signaling. *Curr. Opin. Plant Biol.* **50**, 18–28 (2019).
4. Monteiro, F. & Nishimura, M. T. Structural, functional, and genomic diversity of plant NLR proteins: an evolved resource for rational engineering of plant immunity. *Annu. Rev. Phytopathol.* **56**, 243–267 (2018).
5. Lapin, D., Bhandari, D. D. & Parker, J. E. Origins and immunity networking functions of EDS1 family proteins. *Annu. Rev. Phytopathol.* **58**, 253–276 (2020).
6. Feehan, J. M., Castel, B., Bentham, A. R. & Jones, J. D. Plant NLRs get by with a little help from their friends. *Curr. Opin. Plant Biol.* **56**, 99–108 (2020).
7. Yuan, M. et al. Pattern-recognition receptors are required for NLR-mediated plant immunity. *Nature* **592**, 105–109 (2021).
8. Ngou, B. P. M., Ahn, H. K., Ding, P. & Jones, J. D. G. Mutual potentiation of plant immunity by cell-surface and intracellular receptors. *Nature* **592**, 110–115 (2021).
9. Wan, W. L. et al. Comparing *Arabidopsis* receptor kinase and receptor protein-mediated immune signaling reveals BIK1-dependent differences. *New Phytol.* **221**, 2080–2095 (2019).
10. Rao, S. et al. Roles of receptor-like cytoplasmic kinase VII members in pattern-triggered immune signaling. *Plant Physiol.* **177**, 1679–1690 (2018).
11. Zhang, L. et al. Distinct immune sensors for fungal endopolygalacturonases in closely related Brassicaceae. *Nat. Plants*, https://doi.org/10.1038/s41477-021-00982-2 (2021).
12. Fan, L. et al. Genotyping-by-sequencing-based identification of *Arabidopsis* pattern recognition receptor RLP32 recognizing proteobacterial translation initiation factor IF1. Preprint at https://doi.org/10.1101/2021.03.04.433884 (2021).
13. Böttcher, C. et al. The multifunctional enzyme CYP71B15 (PHYTOALEXIN DEFICIENT3) converts cysteine-indole-3-acetonitrile to camalexin in the indole-3-acetonitrile metabolic network of *Arabidopsis thaliana*. *Plant Cell* **21**, 1830–1845 (2009).
14. Mishina, T. E. & Zeier, J. The *Arabidopsis* flavin-dependent monooxygenase FMO1 is an essential component of biologically induced systemic acquired resistance. *Plant Physiol.* **141**, 1666–1675 (2006).
15. Böhm, H. et al. A conserved peptide pattern from a widespread microbial virulence factor triggers pattern-induced immunity in *Arabidopsis*. *PLoS Pathog.* **10**, e1004491 (2014).
16. Sun, X. et al. Pathogen effector recognition-dependent association of NRG1 with EDS1 and SAG101 in TNL receptor immunity. *Nat. Commun.* **12**, 3335 (2021).
17. Lapin, D. et al. A coevolved EDS1–SAG101–NRG1 module mediates cell death signaling by TIR-domain immune receptors. *Plant Cell* **31**, 2430–2455 (2019).
18. Cui, H. et al. A core function of EDS1 with PAD4 is to protect the salicylic acid defense sector in *Arabidopsis* immunity. *New Phytol.* **213**, 1802–1817 (2017).
19. Wagner, S. et al. Structural basis for signaling by exclusive EDS1 heteromeric complexes with SAG101 or PAD4 in plant innate immunity. *Cell Host Microbe* **14**, 619–630 (2013).
20. Bhandari, D. D. et al. An EDS1 heterodimer signalling surface enforces timely reprogramming of immunity genes in *Arabidopsis*. *Nat. Commun.* **10**, 772 (2019).
21. Joglekar, S. et al. Chemical activation of EDS1/PAD4 signaling leading to pathogen resistance in *Arabidopsis*. *Plant Cell Physiol.* **59**, 1592–1607 (2018).
22. Saile, S. C. et al. Two unequally redundant "helper" immune receptor families mediate *Arabidopsis thaliana* intracellular "sensor" immune receptor functions. *PLoS Biol.* **18**, e3000783 (2020).
23. Reuter, L. et al. Light-triggered and phosphorylation-dependent 14-3-3 association with NONPHOTOTROPIC HYPOCOTYL 3 is required for hypocotyl phototropism. Preprint at https://doi.org/10.1101/2021.04.09.439179 (2021).
24. Koenig, D. et al. Long-term balancing selection drives evolution of immunity genes in *Capsella*. *eLife* **8**, e43606 (2019).
25. Guo, Y. L. et al. Genome-wide comparison of nucleotide-binding site-leucine-rich repeat-encoding genes in *Arabidopsis*. *Plant Physiol.* **157**, 757–769 (2011).
26. 1001 Genomes Consortium. 1,135 Genomes reveal the global pattern of polymorphism in *Arabidopsis thaliana*. *Cell* **166**, 481–491 (2016).
27. Cao, J. et al. Whole-genome sequencing of multiple *Arabidopsis thaliana* populations. *Nat. Genet.* **43**, 956–963 (2011).
28. Lin, Z. J., Liebrand, T. W., Yadeta, K. A. & Coaker, G. PBL13 is a serine/threonine protein kinase that negatively regulates *Arabidopsis* immune responses. *Plant Physiol.* **169**, 2950–2962 (2015).
29. Thomma, B. P., Nürnberger, T. & Joosten, M. H. Of PAMPs and effectors: the blurred PTI–ETI dichotomy. *Plant Cell* **23**, 4–15 (2011).
30. Gust, A. A., Pruitt, R. & Nürnberger, T. Sensing danger: key to activating plant immunity. *Trends Plant Sci.* **22**, 779–791 (2017).

Methods

Plant material

All *Arabidopsis* mutants used in this study were in the *A. thaliana* Col-0 ecotype and are listed in Supplementary Table 3. Complemented transgenic lines and their respective mutant backgrounds are described in Supplementary Table 3. *Arabidopsis* plants were grown in soil in climate chambers under short day conditions (8 h/16 h (light/dark), 150 µmol m^{-2} s^{-1} white fluorescent light, 40–60% humidity, 22 °C). *N. benthamiana* wild-type plants were grown in soil in either a greenhouse or climate chambers under 12 h/12 h light/dark cycle at 60–70% humidity and 24–26 °C.

Elicitors used in this study

Flg22, elf18, nlp20 and pg13(At) peptides were synthesized according to the published sequences[11,15,31,32] by Genscript, prepared as 10 mM stock solutions in DMSO and diluted in ddH$_2$O before use. Full-length IF1 from *Escherichia coli* was synthesized by Genscript as a biotinylated fusion protein and resuspended in ddH$_2$O as a 1 mM stock solution[12]. The RLP1 elicitor eMax was originally identified in *Xanthomonas*[33]. We found that eMax is also present in other Proteobacteria including *Lysobacter*. Here we used eMax partially purified from the *Lysobacter* strain Root690 (ref. [34]). *Lysobacter* was grown in SOB medium overnight at 28 °C with shaking at 200 r.p.m. and collected by centrifugation. The pellet was resuspended in 50 mM MES, pH 5.7, and 50 mM NaCl, and cells were lysed by sonication, after which the supernatant was fractionated using a HiTrapQ FF (Cytiva) anion-exchange column. An eMax-containing fraction with high ethylene-inducing activity on *fls2 efr* leaves, but no activity on *rlp1* leaves[33] was used for the RLCK-VII mutant screen as shown in Extended Data Fig. 1a.

Measurement of ethylene production

Leaves of 6-week-old *Arabidopsis* plants were cut into pieces (about 0.5 × 0.5 cm) and floated on H$_2$O overnight. For Extended Data Fig. 4c, leaves were floated on either water or 100 nM thaxtomin A. Three leaf pieces were incubated in a sealed 6.5-ml glass tube with 0.4 ml of 50 mM MES buffer, pH 5.7, and the indicated elicitor. Ethylene accumulation was measured after 4 h by gas chromatographic analysis (GC-14A; Shimadzu) of 1 ml of the air drawn from the closed tube with a syringe.

Measurement of ROS production

ROS assays were performed as previously described[31,35]. Leaves of 5-week-old *Arabidopsis* plants were cut into pieces of equal size and floated on H$_2$O overnight. One leaf piece per well was transferred to a 96-well plate containing 20 µM L-012 (Wako Pure Chemical Industries) and 2 µg ml^{-1} peroxidase. Luminescence was measured over 1 h following elicitation or mock treatment using a Mithras LB 940 luminometer (Berthold Technologies). Total relative light unit production was determined by calculating the area under the scatter curve for 30 min post-elicitation.

Measurement of elicitor-induced callose deposition

Leaves of 5-week-old *Arabidopsis* plants were infiltrated with 500 nM elicitor and incubated for 16 h. Leaves were bleached with 95% ethanol and stained with aniline blue as described[36]. Images were collected at a magnification of ×64 on an AxioZoom.V16 microscope equipped with an AxioCam503 colour camera (Zeiss) and a DAPI filter (excitation filter: 390 nM, emission filter: 460 nM) using ZenBlue software. Image colours were inverted and converted to black and white. Black pixels indicating callose were counted with ImageJ.

MAPK activation

Arabidopsis leaves (4.5–6-week old) were infiltrated with water, 1 or 0.5 µM nlp20, or 1 µM flg22. At the indicated time points, leaves were harvested and frozen in liquid nitrogen. MAPK activation was assessed by blotting with a phospho-specific p44-p42 antibody (1:3,000; Cell Signaling) as previously described[37].

Seedling growth inhibition

Sterilized seeds were placed on ½ MS plates (1% sucrose, 0.8% agar). After vernalization, seeds were incubated in a long day chamber (16 h/8 h (light/dark), 150 µmol m^{-2} s^{-1} white fluorescent light, 22 °C). After 5 d, seedlings were transferred to ½ MS with 1% sucrose, 10 mM NaCl, 0.01% BSA and 100 nM elf18 or flg22. After 7 d, seedlings were blotted dry and fresh weight was measured. Nlp20 does not cause seedling growth inhibition and thus was not tested here[15].

Quantitative reverse transcription PCR

Leaves from 6-week-old *Arabidopsis* plants were infiltrated with water (mock) or the indicated elicitors. Total RNA was isolated from leaves harvested at the indicated time point using the NucleoSpin RNA Plus Kit (Macherey-Nagel). cDNA was synthesized from 2 µg of total RNA using the RevertAid First Strand cDNA Synthesis Kit (Thermo Scientific). Quantitative PCRs and measurements were performed with a CFX384 Real-Time PCR detection system or an iQ5 Multi-Colour Real-Time PCR detection system (Bio-Rad) using the SYBR Green Fluorescein Mix (Thermo Scientific) and the primers listed in Supplementary Table 4. Transcript levels of target genes were normalized to the transcript levels of the housekeeping genes *EF1a* or *UBIQUITIN 5*.

Pathogenicity assays

Pst DC3000 inoculations were performed as described[15]. For induced resistance assays, leaves of 4–6-week-old *Arabidopsis* plants were infiltrated with 1 µM nlp20, 1 µM flg22 or mock-treated 24 h before bacterial infection. Leaves were infiltrated with *Pst* DC3000 or *Pst* DC3000 AvrRPS4 at a density of 10^4 cell per ml and bacterial growth was quantified after 3 d.

Cloning of recombinant PBL31

PBL31 and *PBL31*^{K201A} were cloned into pDEST15 and transformed into BL21-AI (Thermo Scientific). Cultures were grown at 37 °C to OD$_{600}$ = 0.3 and then transferred to 17 °C. Expression was induced with 0.2% L-arabinose when the culture reached OD$_{600}$ = 0.6 and incubated overnight. The recombinant proteins were purified by immobilized metal ion affinity chromatography using a HisTrap HP column (Cytiva) and then dialysed against 20 mM Tris, pH 8, and 100 mM NaCl. Proteins were diluted to 0.25 mg ml^{-1} and treated with 200 U ml^{-1} calf intestinal phosphatase (Sigma) or mock-treated for 3 h at 37 °C in the presence of 1× calf intestinal phosphatase buffer (Sigma). Samples were analysed by anti-His protein blot (Abcam).

N. benthamiana and *Arabidopsis* IPs and protein blotting

Leaves of *N. benthamiana* were transiently transformed with the indicated constructs and harvested after 2–3 d. For the elicitor-treated samples, leaves were infiltrated with water or 1 µM nlp20 10 min before harvesting. IPs were performed with 200–250 mg of tissue. Tagged proteins were immunoprecipitated for 1 h at 4 °C using GFP-Trap beads (ChromoTek) as previously described[38,39]. Protein blotting was performed using antibodies to GFP (1:4,000; Torrey Pines Biolabs), HA (1:2,000; Sigma) or Myc (1:5,000; Sigma). For Extended Data Fig. 7b, d, protein blotting was performed using antibodies to GFP (1:1,500; Roche) and HA (1:2,000; Roche).

Immunoblotting was used to check the background levels of FLS2 (1:2,000; Agrisera), BAK1 (1:10,000; Agrisera), MPK3 (1:5,000; Sigma), MPK4 (1:1,000; Sigma) and MPK6 (1:1,000; Sigma) in 5–6-week-old *Arabidopsis*. For split luciferase (Luc) experiments, protein abundance was checked with Luc and CLuc antibodies (1:5,000; Sigma). *Arabidopsis* plants (4.5-week old) containing *p35S::StrepII-3×HA-YFP* (Col-0), *pPAD4::YFP-PAD4* (*pad4-1 sag101-3* background) or *pSAG101::SAG101-YFP* (*pad4-1 sag101-3* background) were

syringe-infiltrated with mock (DMSO) or 0.5 µM nlp20 and harvested after 10 min or 3 h. Protein extraction and IP using anti-GFP agarose beads (Chromotek) were performed as previously described[16]. Protein quality in inputs was checked on immunoblots (Extended Data Fig. 9c) using antibodies to GFP (1:2,500; Roche).

Ratiometric bimolecular fluorescence complementation
The coding sequences of SOBIR1, ADR1, ADR1-L1 and ADR1-L2 were cloned into the 2in1 bimolecular fluorescence complementation CC gateway-compatible destination vector[40,41]. Destination vectors were transiently expressed in *N. benthamiana*, and complementation of YFP was analysed at 24 h after infection with the confocal laser scanning microscope LSM880 (Zeiss) using a ×63 water-immersion objective. Settings were as follows: YFP was excited using a 514-nm laser, collecting emission between 516 and 556 nm; RFP was excited using a 561-nm laser with an emission spectrum of 597–634 nm. Images were processed with ZENblue software (Zeiss) for adjustment of brightness and contrast.

Split Luc assays
Firefly Luc complementation assays were performed as previously described[42]. In brief, the cDNA of indicated genes were amplified and cloned into 35S-pCAMBIA1300-Nluc or 35S-pCAMBIA1300-Cluc. The *A. tumefaciens* strain GV3101 carrying these plasmids was infiltrated into *N. benthamiana* leaves. After 48 h of infiltration, leaf discs were taken and incubated with 1 mM luciferin in a 96-well plate. The Luc activity was measured by the EnSpire Multimode Plate Reader (Perkin Elmer). Protein expression was detected by immunoblot against CLuc and Luc (Sigma) (Extended Data Fig. 7f).

FRET-FLIM
For FRET-FLIM analysis, C-terminal GFP fusions of SOBIR1 (pSol2095)[43] and PBL31 (in PGWB5 (ref. [44])) were used as donor constructs. C-terminal RFP fusions of SOBIR1, PBL31, PAD4, EDS1, SAG101, ADR1, ADR1-L1 and ADR1-L2 (in pB7RWG2 (ref. [45])) were used as acceptors. N-terminally tagged RFP–NPH3^{S744A} (in pB7WGR2 (refs. [23,45])) served as a plasma membrane-associated control; the S744A mutation blocks light-triggered dissociation from the plasma membrane[23]. EDS1–HA and PAD4–HA were expressed from pGWB14 (ref. [44]). These binary vectors and a p19-expressing construct as silencing inhibitor were transformed into the *A. tumefaciens* strain GV3101. For transformation of *N. benthamiana* leaves, *Agrobacterium* cultures were adjusted to an OD_{600} of 0.2 in infiltration medium, and a 1:1:1(:1) mixture was infiltrated into leaves of 3–4-week-old plants. FLIM measurements were performed, according to a modified protocol of ref. [46], 26–48 h after infiltration on a SP8 confocal laser scanning microscope (Leica Microsystems) with Leica Microsystems Application Suite software and a FastFLIM upgrade from PicoQuant consisting of Sepia Multichannel Picosecond Diode Laser, PicoQuant Timeharp 260, TCSPC Module and Picosecond Event Timer (Picoquant). Imaging was done by using a ×63/1.20 water-immersion objective and focusing on the plasma membrane of the abaxial epidermal cells. The presence of the fluorophores was shown by excitation with 488 nm or 561 nm, and 500–550-nm or 600–650-nm detection range for GFP or RFP, respectively. HA-tagged proteins were detected by western blot analysis. Colocalization was demonstrated by reading out signal intensities over the plasma membrane. As laser power and gain were varied, the intensities do not reflect the absolute expression levels towards each other but validate the colocalization at the plasma membrane. The GFP FLT τ [ns] in cells co-expressing different constructs was determined by excitation with a pulsed laser with a 470-nm wavelength and a repetition rate of 40 MHz. The maximal count rate was set to about 10,000 kCnts s^{-1} and photons were collected until 500 photons in the brightest pixel were reached at a resolution of 256 × 256 pixels. Data processing was performed with SymPhoTime software. A region of interest covering the plasma membrane was defined and FLT

[ns] was determined by biexponential curve fitting and a correction for the instrument response function.

FRET-FLIM data are derived from at least three independent biological replicates with a total sample size of $n \geq 11$ per FRET pair or donor-only control. All sample numbers and statistical analysis data can be found in Supplementary Table 5. As cell death, which was a problem in several co-expression combinations, correlates with high A[2] values, samples were only included in the analysis when the A[1] [kCnts] to A[2] [kCnts] ratio was above 1; the other measurements were discarded. As data were not equally distributed, a Wilcoxon or Kruskal–Wallis test was performed, followed by a post-hoc test (Steel–Dwass all-pairs comparison).

Preparation of peptides for LC–MS/MS, data acquisition and data analyses
Proteins (from GFP-trap enrichment) were submitted to an on-bead digestion. In brief, dry beads were re-dissolved in 25 µl digestion buffer 1 (50 mM Tris, pH 7.5, 2 M urea, 1 mM DTT and 5 ng µl^{-1} trypsin) and incubated for 30 min at 30 °C in a Thermomixer with 400 r.p.m. Next, beads were pelleted and the supernatant was transferred to a fresh tube. Digestion buffer 2 (50 mM Tris, pH 7.5, 2 M urea and 5 mM CAA) was added to the beads. After mixing, the beads were pelleted and supernatants were collected. Combined supernatants were incubated overnight at 32 °C in a Thermomixer with 400 r.p.m.; samples were protected from light during incubation. The digestion was stopped by adding 1 µl TFA and desalted with C18 Empore disc membranes according to the StageTip protocol[47]. Dried peptides were re-dissolved in 2% ACN and 0.1% TFA (10 µl) and diluted to 0.2 µg µl^{-1} for analysis. Samples were analysed using an EASY-nLC 1000 (Thermo Fisher) coupled to a Q Exactive mass spectrometer (Thermo Fisher). Peptides were separated on 16-cm fritless silica emitters (New Objective; with an inner diameter of 75 µm), packed in-house with reversed-phase ReproSil-Pur C18 AQ 1.9 µm resin (Dr. Maisch). Peptides were loaded on the column and eluted for 115 min using a stepwise linear gradient of 5% to 95% solvent B (0–5 min, 0-5% B; 5–65 min, 5-20% B; 65–90 min, 20-35% B; 90–100 min, 35-55% B; 100–105 min, 55-95% B; 105–115 min, 95% B) (solvent A 0% ACN and 0.1% FA; solvent B 80% ACN and 0.1% FA) at a flow rate of 300 nl min^{-1}. Mass spectra were acquired in data-dependent acquisition mode with a TOP15 method. MS spectra were acquired in the Orbitrap analyser with a mass range of 300–1,750 m/z at a resolution of 70,000 FWHM and a target value of 3×10^6 ions. Precursors were selected with an isolation window of 2.0 m/z. HCD fragmentation was performed at a normalized collision energy of 25. MS/MS spectra were acquired with a target value of 10^5 ions at a resolution of 17,500 FWHM, a maximum injection time of 55 ms and a fixed first mass of m/z 100. Peptides with a charge of +1, greater than 6 or with unassigned charge state were excluded from fragmentation for MS2; dynamic exclusion for 30 s prevented repeated selection of precursors. Raw data were processed using MaxQuant software (version 1.6.3.4; http://www.maxquant.org/)[48] with label-free quantification (LFQ) and iBAQ enabled[49]. MS/MS spectra were searched by the Andromeda search engine against a combined database containing the sequences from *A. thaliana* (TAIR10_pep_20101214; https://www.arabidopsis.org/download/index-auto. jsp?dir=%2Fdownload_files%2FProteins%2FTAIR10_protein_lists) and sequences of 248 common contaminant proteins and decoy sequences. Trypsin specificity was required and a maximum of two missed cleavages were allowed. The minimal peptide length was set to seven amino acids. Carbamidomethylation of cysteine residues was set as fixed, and oxidation of methionine and protein N-terminal acetylation were set as variable modifications. Peptide spectrum matches and proteins were retained if they were below a false discovery rate of 1%. Statistical analysis of the MaxLFQ values was carried out using Perseus (version 1.5.8.5; http://www.maxquant.org/). Quantified proteins were filtered for reverse hits and hits 'identified by site', and MaxLFQ values were log$_2$ transformed. After grouping samples by condition, only those proteins that had three valid

values in one of the conditions were retained for the subsequent analysis. Two-sample t-tests were performed using a permutation-based false discovery rate of 5%. Alternatively, quantified proteins were grouped by condition and only those hits that had four valid values in one of the conditions were retained. Missing values were imputed from a normal distribution (1.8 downshift, separately for each column). Volcano plots were generated in Perseus using a false discovery rate of 0.05 and an S0 = 1. The Perseus output was exported and further processed using Excel (Supplementary Tables 1, 2). The MS proteomics data have been deposited to the ProteomeXchange Consortium[50] via the PRIDE[51] partner repository with the dataset identifier PXD026120.

Conservation analysis of LRR-RKs, LRR-RPs and NLRs in *Arabidopsis*

Illumina reads from 80 *Arabidopsis* accessions from the first phase study of the 1001 Genomes project[26,27] were mapped to the reference genome of Col-0 using version 0.7.15-r1140 of the BWA-backtrack algorithm[52] with parameters: $k = 1$ in bwa aln command; $n = 10,000$; with the maximal number of mismatches allowed being 1. Paired-end information was discarded. The TAIR10 assembly of the *Arabidopsis* Col-0 genome was used for the reference genome (https://arabidopsis.org). The output mapped files were processed with samtools mpileup version 1.9 (ref. [53]); parameters: aa; $d = 10,000$; $Q = 0$. A total list of 163 NLR genes was used in the analysis, which was based on 159 NLR genes previously identified[25] and 4 additional, manually curated genes (*AT1G63860*, *AT1G72920*, *AT1G72930* and *AT5G45230*). The coding sequence (CDS) portions of the genes were extracted, defined as the union of all the CDS models of the gene based on the TAIR10 annotation. Fractions of the CDS sequence with non-zero coverage were calculated for each gene–accession combination (hereafter known as 'coverage fractions'). Genes were assigned into conserved, complex and presence/absence categories using a threshold-based approach. To define thresholds, k means algorithm was initiated with three centres at 0, 0.5 and 1 and applied to the coverage fractions, resulting in thresholds at 0.37 and 0.81. Coverage fractions were then discretized by applying these thresholds into 'absent', 'intermediate' and 'present' categories, from lowest to highest values. NLR genes were assigned as conserved if there were no accessions with 'absent' coverage and at least 95% of all accessions had high coverage. Genes with more than 5% of accessions having 'intermediate' coverage values were assigned as complex, and genes that were absent in at least one accession not classified as complex, were assigned as presence/absence. This procedure was also applied to LRR-RP-encoding genes[54] and LRR-RK-encoding genes[55]. The conserved category does not necessarily imply functional or structural conservation but is used in the genomic sense to indicate sequence conservation, as measured by the presence of sub-sequences whose identities are within the applied thresholds.

Data analysis

No statistical methods were used to predetermine sample size. The experiments were not randomized. The investigators were not blinded to allocation during experiments and outcome assessment. Data were plotted using R Studio (https://www.r-project.org/) or Microsoft Office Excel. Data were represented as the mean ± s.e.m. or as box-and-whisker plots in which the centre line indicates the median, the bounds of the box indicate the 25th and 75th percentiles, and the whiskers indicate 1.5 × the interquartile range between the 25th and the 75th percentile. Statistical analyses were performed using R Studio/R or JMP (SAS). Unless otherwise stated, graphs present data from a single experiment. Data were tested for normal distribution with Shapiro–Wilk test and equal variance with Fligner–Killeen (R) or Levene's test (JMP). Data with non-normal distribution were tested for significant differences using two-sided Wilcoxon rank-sum test with continuity correction (for two groups) or Kruskal–Wallis test with a post-hoc two-sided Steel–Dwass test (for more than two groups). For Extended Data Fig. 1a, the

Steel–Dwass test revealed no significant differences between genotypes as this test is very stringent with large group sizes and small sample numbers (n). We therefore further performed two-sided Wilcoxon rank-sum pairwise tests, which are not affected by group size. Data with normal distribution were analysed with a two-sided Student's t-test or, if variances were unequal, a two-sided Welch's t-test. A summary of statistical analyses is provided in Supplementary Table 5. Data and statistical analysis for MS analyses are provided in Supplementary Tables 1, 2.

Reporting summary

Further information on research design is available in the Nature Research Reporting Summary linked to this paper.

Data availability

All data are available within this article and its Supplementary Information. Proteomics data are available via the ProteomeXchange Consortium with the identifier PXD026120. MS data were searched against a combined database containing protein sequences from *A. thaliana* TAIR10_pep_20101214 (https://www.arabidopsis.org/download/index-auto.jsp?dir=%2Fdownload_files%2FProteins%2FTAIR10_protein_lists). Genomics data from *A. thaliana* accessions were obtained from the 1001 Genomes project (https://1001genomes.org/data-center.html) and mapped to the TAIR10 assembly of the genome (https://arabidopsis.org). Original gel blots are shown in Supplementary Fig. 1. Statistical analyses for all quantitative data are provided in Supplementary Tables 1, 2 and 5. Source data are provided with this paper.

31. Felix, G., Duran, J. D., Volko, S. & Boller, T. Plants have a sensitive perception system for the most conserved domain of bacterial flagellin. *Plant J.* **18**, 265–276 (1999).
32. Kunze, G. et al. The N terminus of bacterial elongation factor Tu elicits innate immunity in *Arabidopsis* plants. *Plant Cell* **16**, 3496–3507 (2004).
33. Jehle, A. K. et al. The receptor-like protein ReMAX of *Arabidopsis* detects the microbe-associated molecular pattern eMax from *Xanthomonas*. *Plant Cell* **25**, 2330–2340 (2013).
34. Bai, Y. et al. Functional overlap of the *Arabidopsis* leaf and root microbiota. *Nature* **528**, 364–369 (2015).
35. Albert, M. et al. Regulation of cell behaviour by plant receptor kinases: pattern recognition receptors as prototypical models. *Eur. J. Cell Biol.* **89**, 200–207 (2010).
36. Jin, L. & Mackey, D. M. Measuring callose deposition, an indicator of cell wall reinforcement, during bacterial infection in *Arabidopsis*. *Methods Mol. Biol.* **1578**, 195–205 (2017).
37. Willmann, R., Haischer, D. J. & Gust, A. A. Analysis of MAPK activities using MAPK-specific antibodies. *Methods Mol. Biol.* **1171**, 27–37 (2014).
38. Chinchilla, D. et al. A flagellin-induced complex of the receptor FLS2 and BAK1 initiates plant defence. *Nature* **448**, 497–500 (2007).
39. El Kasmi, F. et al. Signaling from the plasma-membrane localized plant immune receptor RPM1 requires self-association of the full-length protein. *Proc. Natl Acad. Sci. USA* **114**, E7385–E7394 (2017).
40. Grefen, C. & Blatt, M. R. A. A 2in1 cloning system enables ratiometric bimolecular fluorescence complementation (rBiFC). *Biotechniques* **53**, 311–314 (2012).
41. Mehlhorn, D. G., Wallmeroth, N., Berendzen, K. W. & Grefen, C. 2in1 vectors improve in planta BiFC and FRET analyses. *Methods Mol. Biol.* **1691**, 139–158 (2018).
42. Chen, H. et al. Firefly luciferase complementation imaging assay for protein–protein interactions in plants. *Plant Physiol.* **146**, 323–324 (2008).
43. Liebrand, T. W. et al. Receptor-like kinase SOBIR1/EVR interacts with receptor-like proteins in plant immunity against fungal infection. *Proc. Natl Acad. Sci. USA* **110**, 10010–10015 (2013).
44. Nakagawa, T. et al. Development of series of gateway binary vectors, pGWBs, for realizing efficient construction of fusion genes for plant transformation. *J. Biosci. Bioeng.* **104**, 34–41 (2007).
45. Karimi, M., Inzé, D. & Depicker, A. GATEWAY vectors for *Agrobacterium*-mediated plant transformation. *Trends Plant Sci.* **7**, 193–195 (2002).
46. Glöckner, N. et al. Three-fluorophore FRET enables the analysis of ternary protein association in living plant cells. Preprint at https://doi.org/10.1101/722124 (2020).
47. Rappsilber, J., Ishihama, Y. & Mann, M. Stop and go extraction tips for matrix-assisted laser desorption/ionization, nanoelectrospray, and LC/MS sample pretreatment in proteomics. *Anal. Chem.* **75**, 663–670 (2003).
48. Cox, J. & Mann, M. MaxQuant enables high peptide identification rates, individualized p.p.b.-range mass accuracies and proteome-wide protein quantification. *Nat. Biotechnol.* **26**, 1367–1372 (2008).
49. Tyanova, S., Temu, T. & Cox, J. The MaxQuant computational platform for mass spectrometry-based shotgun proteomics. *Nat. Protoc.* **11**, 2301–2319 (2016).
50. Deutsch, E. W. et al. The ProteomeXchange consortium in 2020: enabling 'big data' approaches in proteomics. *Nucleic Acids Res.* **48**, D1145–D1152 (2020).
51. Perez-Riverol, Y. et al. The PRIDE database and related tools and resources in 2019: improving support for quantification data. *Nucleic Acids Res.* **47**, D442–D450 (2019).

52. Li, H. & Durbin, R. Fast and accurate short read alignment with Burrows–Wheeler transform. *Bioinformatics* **25**, 1754–1760 (2009).
53. Li, H. et al. The Sequence Alignment/Map format and SAMtools. *Bioinformatics* **25**, 2078–2079 (2009).
54. Wang, G. et al. A genome-wide functional investigation into the roles of receptor-like proteins in *Arabidopsis*. *Plant Physiol.* **147**, 503–517 (2008).
55. Shiu, S. H. et al. Comparative analysis of the receptor-like kinase family in *Arabidopsis* and rice. *Plant Cell* **16**, 1220–1234 (2004).
56. Kurup, S. et al. Marking cell lineages in living tissues. *Plant J.* **42**, 444–453 (2005).

Competing interests The authors declare no competing interests.

Additional information
Supplementary information The online version contains supplementary material available at https://doi.org/10.1038/s41586-021-03829-0.
Correspondence and requests for materials should be addressed to Jane E. Parker or Thorsten Nürnberger.
**Peer review information** *Nature* thanks Gitta Coaker and the other, anonymous, reviewer(s) for their contribution to the peer review of this work. Peer reviewer reports are available.
**Reprints and permissions information** is available at http://www.nature.com/reprints.
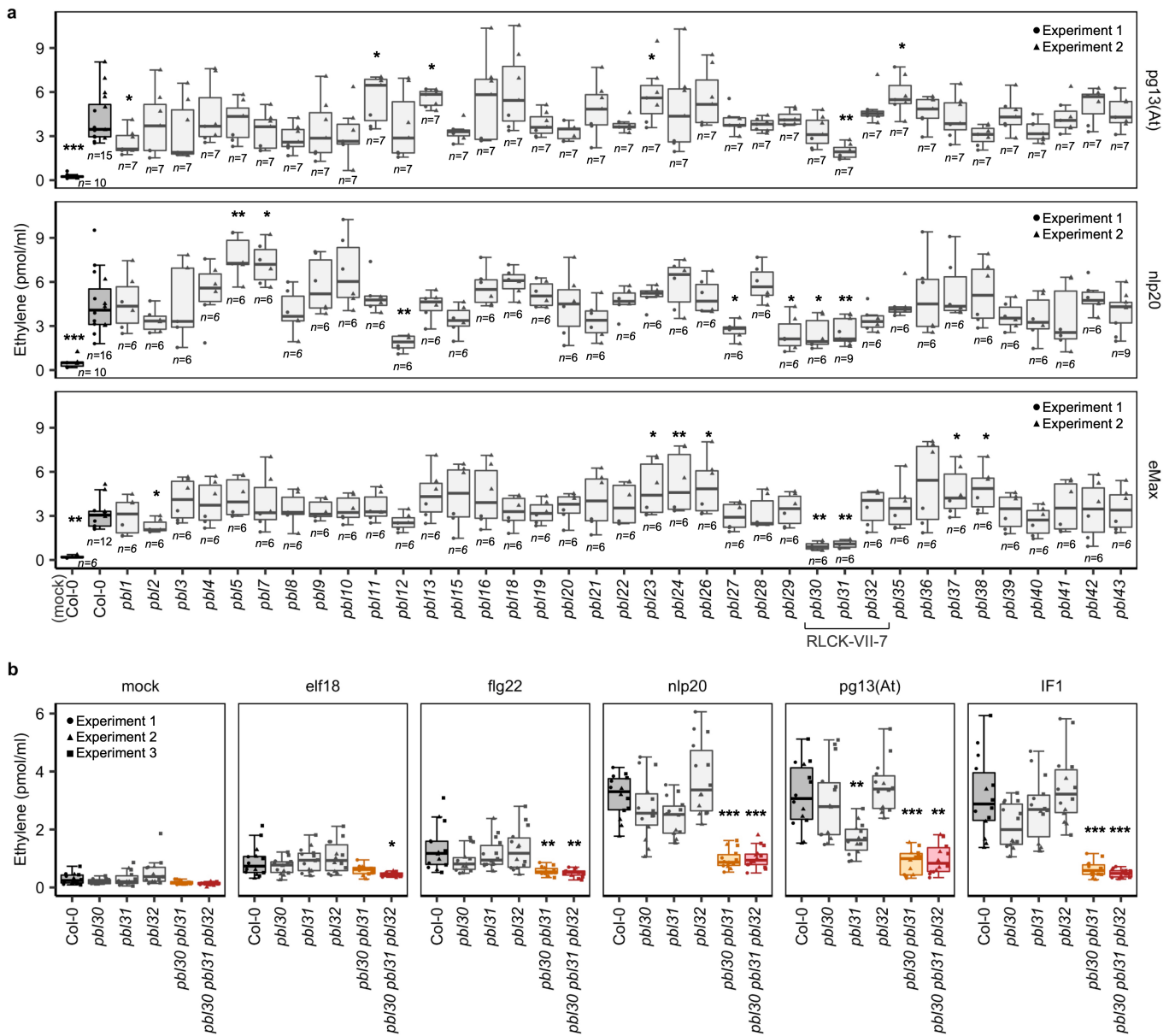
Extended Data Fig. 1 | LRR-RP-mediated ethylene responses are dependent on RLCK-VII-7 kinases PBL30 and PBL31. a, RLCK-VII mutant screen for positive regulators of LRR-RP signalling. $n \geq 6$, each from 3 leaf pieces. Exact n values are shown in the graph. Data are from 2 independent experiments. Two-sided Wilcoxon rank sum pairwise tests with continuity correction were used to analyse significant differences between elicitor-treated Col-0 and the indicated mutant (*$P \leq 0.05$, **$P \leq 0.01$). **b**, Elicitor-induced ethylene production in Col-0 and RLCK-VII-7 mutants. $n = 14$, each from 3 leaf pieces. Data are from 3 independent experiments. Statistical differences between Col-0 and the indicated mutants were analysed using a Kruskal–Wallis test with a post hoc two-sided Steel-Dwass test (*$P \leq 0.05$, **$P \leq 0.01$, ***$P \leq 0.0001$). Centre line: median, bounds of box: 25th and 75th percentiles, whiskers: 1.5*IQR (IQR: the interquartile range between the 25th and the 75th percentile). Exact P values for all experiments are provided in Supplementary Table 5.
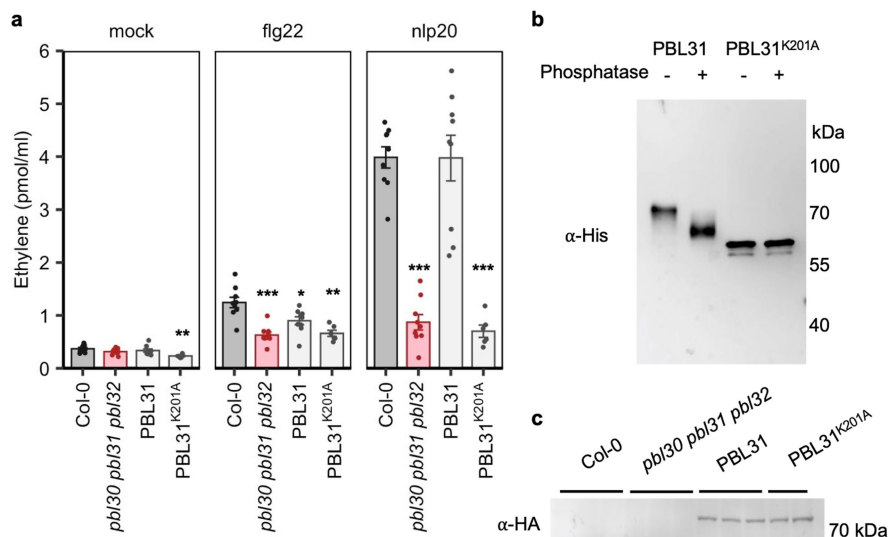
Extended Data Fig. 2 | PBL31 activity in RLP23 signalling requires its kinase activity. a, Ethylene accumulation in *pbl30 pbl31 pbl32* complemented with wild-type PBL31-HA (PBL31) or the kinase-dead variant PBL31^K201A-HA (PBL31^K201A). Bars indicate mean ethylene response ± s.e.m. For PBL31^K201A, *n* = 6; for all others, *n* = 9. A two-sided Welch's *t*-test was used to analyse significant differences between Col-0 and the indicated line for the given elicitor treatment (**$P \le 0.01$, ***$P \le 0.0001$). Exact *P* values are provided in Supplementary Table 5. The experiment was repeated 3 times with similar results. **b**, PBL31 has autokinase activity that is abolished in the PBL31^K201A mutant. Recombinant PBL31 and PBL31^K201A were subjected to SDS–PAGE followed by anti-His protein blot. PBL31^K201A runs near the predicted position for the tagged protein (57.4 kDa). The wild-type version migrates more slowly, consistent with it being auto-phosphorylated. Phosphorylation of the wild-type PBL31 was confirmed by treatment with calf intestinal phosphatase, which increased the migration rate of PBL31 but not PBL31^K201A. The experiment was repeated 2 times with similar results. **c**, Anti-HA protein blot with material from plants used in **a**. For gel source data, see Supplementary Fig. 1.
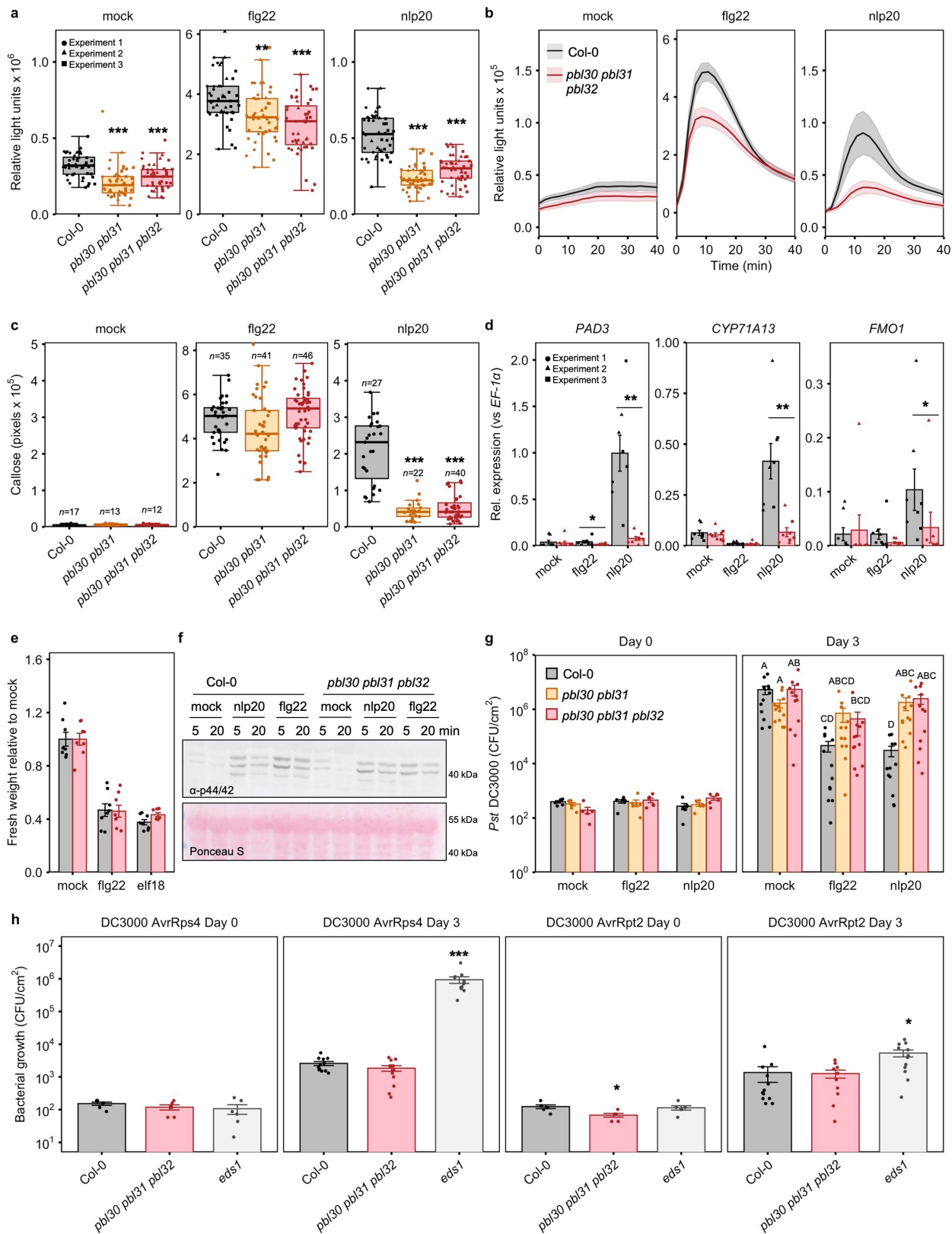
Extended Data Fig. 3 | See next page for caption.

Extended Data Fig. 3 | Immune responses of RLCK-VII-7 mutants treated with LRR-RP-recognized and LRR-RK-recognized elicitors. a, b, Elicitor-induced ROS production is impaired in *pbl30 pbl31 pbl32*. **a,** Total elicitor-induced ROS production over 30 min in Col-0, *pbl30 pbl31*, and *pbl30 pbl31 pbl32*. $n = 48$ leaf pieces from 3 independent experiments. For all panels *pbl30 pbl31* is in orange, *pbl30 pbl31 pbl32* is in pink. For **a, c, h,** statistical differences between Col-0 and the indicated mutants were analysed using a Kruskal–Wallis test with a post hoc two-sided Steel-Dwass test (*$P \leq 0.05$, **$P \leq 0.01$, ***$P \leq 0.0001$). **b,** Mean ROS production over time. Solid line, mean; shaded band, s.e.m.; $n = 16$ leaf pieces. **c,** Nlp20-induced callose deposition in Col-0 is dependent on PBL30 and PBL31. $n \geq 12$ images from at least 3 leaves; exact n values are indicated on the graph. **d,** Nlp20-induced expression of *PAD3*, *CYP71A13*, and *FMO1* is impaired in *pbl30 pbl31 pbl32* plants. Bars indicate mean expression relative to *EF-1α* 6 h after mock or elicitor treatment determined by qRT–PCR. $n = 8$ biological replicates from 3 independent experiments. A two-sided Wilcoxon rank sum test with continuity correction was used to analyse significant differences between Col-0 and *pbl30 pbl31 pbl32* for the given elicitor treatment (*$P \leq 0.05$, **$P \leq 0.01$). **e,** Relative fresh weight of 12 d-old Col-0 and *pbl30 pbl31 pbl32* seedlings grown in the presence of flg22 or elf18. No significant differences were observed between Col-0 and *pbl30 pbl31 pbl32* growth for any treatment ($P > 0.05$, two-sided Wilcoxon rank sum test with continuity correction). $n = 8$ biological replicates comprising 2 seedlings; for *pbl30 pbl31 pbl32* treated with elf18, $n = 7$. **f,** MAP kinase activation in Col-0 and *pbl30 pbl31 pbl32* treated with nlp20 or flg22 was analysed by immunoblot assay. Ponceau S-stained RUBISCO large subunit serves as a loading control. For gel source data, see Supplementary Fig. 1. **g,** Elicitor-induced defence against infection is impaired in *pbl30 pbl31* and *pbl30 pbl31 pbl32*. Leaves were infiltrated with the indicated elicitor and challenged with *Pst* DC3000 infection after 24 h. Bacterial colonization was assessed at Day 0 and Day 3. $n = 6$ (Day 0) or 12 (Day 3) biological replicates comprising 2 leaf discs. Bars with different letters indicate significant differences of $P \leq 0.05$ (Kruskal–Wallis test with post hoc two-sided Steel-Dwass test). No statistical differences were observed for Day 0. CFU, colony forming units. **h,** RLCK-VII-7 kinases are not required for an ETI response to *Pst* DC3000 *AvrRps4* or *Pst* DC3000 *AvrRpt2*. $n = 8$ (Day 0) or 12 (Day 3) biological replicates comprising 2 discs; for *pbl30 pbl31 pbl32* infected with *Pst* DC3000 *AvrRpt2* (Day 3), $n = 10$. Growth on *eds1* plants served as control. For box plots in **a, c,** centre line: median, bounds of box: 25th and 75th percentiles, whiskers: 1.5 * IQR. For **d, e, g, h** bars indicate mean ± s.e.m. Experiments in **b, c, e–h** were repeated at least three times with similar results. Exact P values for all quantitative experiments are provided in Supplementary Table 5.
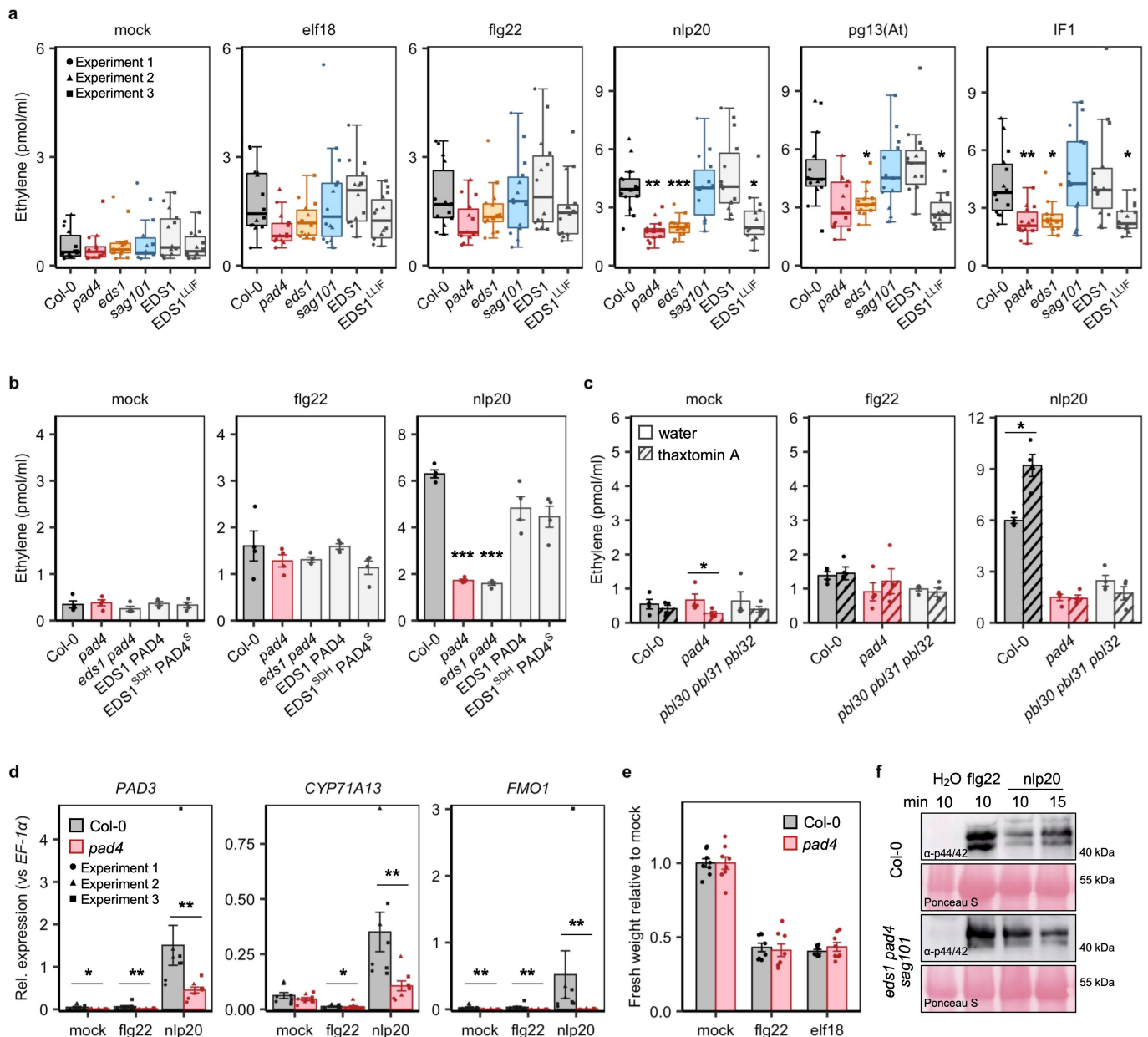
**Extended Data Fig. 4 | PTI responses are partially dependent on PAD4 and EDS1. a**, Elicitor-induced ethylene production in *pad4*, *eds1*, *sag101*, EDS1 and EDS1^LLIF lines. $n = 14$, each from 3 leaf pieces. Data are from 3 independent experiments. Statistical differences between Col-0 and the indicated mutants were analysed using a Kruskal–Wallis test with a post hoc two-sided Steel-Dwass test (*$P \leq 0.05$, **$P \leq 0.01$, ***$P \leq 0.0001$). Centre line: median, bounds of box: 25th and 75th percentiles, whiskers: 1.5 * IQR. **b**, Nlp20-induced ethylene production is not dependent on EDS1 and PAD4 putative lipase activity. The *eds1 pad4* is complemented with wild-type proteins (EDS1 PAD4) or variants harbouring mutations in their putative α/β-hydrolase catalytic residues (EDS1^SDH PAD4^S)[19]. $n = 4$, each from 3 leaf pieces. Statistical differences between Col-0 and the indicated mutants were analysed by two-sided Welch's pairwise tests (**$P \leq 0.01$). For **b**–**e**, bars indicate mean ± s.e.m. **c**, Thaxtomin A pretreatment enhances nlp20-induced ethylene responses in Col-0 but not in *pad4* or *pbl30 pbl31 pbl32* mutants. $n = 4$, each from 3 leaf pieces. Statistical differences between water- and thaxtomin A-treated samples were analysed using a Kruskal–Wallis test with a post hoc two-sided Steel-Dwass test (*$P \leq 0.05$). **d**, Expression of *PAD3*, *CYP71A13* and *FMO1* 6 h after elicitor or mock treatment, determined by qRT–PCR. $n = 8$ biological replicates from 3 independent experiments. A two-sided Wilcoxon rank sum test with continuity correction was used to analyse significant differences between Col-0 and *pad4* for the given elicitor treatment (*$P \leq 0.05$, **$P \leq 0.01$). **e**, Relative fresh weight of 12 d-old Col-0 and *pad4* seedlings grown in the presence of flg22 or elf18. No significant differences were observed between Col-0 and *pad4* growth for any treatment (two-sided Wilcoxon rank sum test with continuity correction). $n = 8$ biological replicates comprising 2 seedlings; for Col-0 treated with elf18, $n = 7$. **f**, MAP kinase activation in Col-0 and *eds1 pad4 sag101* treated with nlp20 or flg22 was analysed by immunoblot assay. Ponceau S-stained RUBISCO large subunit serves as a loading control. For gel source data, see Supplementary Fig. 1. Experiments in **b**–**f** were performed at least three times with similar results. Exact P values for all quantitative experiments are provided in Supplementary Table 5.
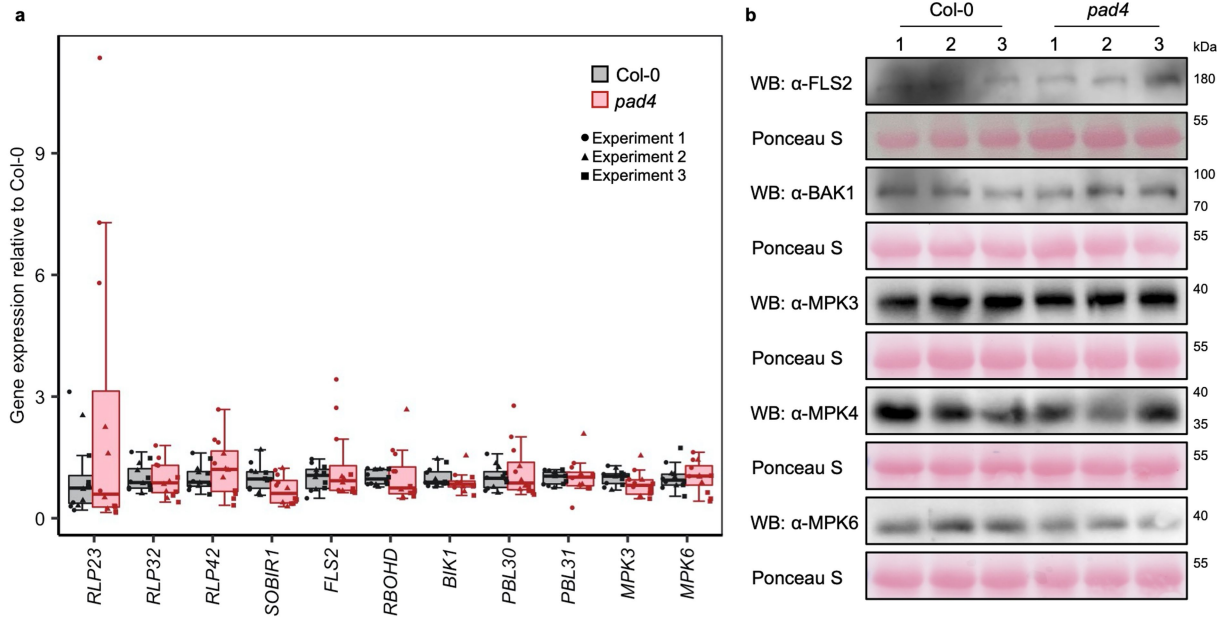
Extended Data Fig. 5 | Transcript and protein levels of immune-related genes in Col-0 and *pad4*. a, Background levels of a set of immune-related genes in naive Col-0 and *pad4*. Relative expression was determined by qRT–PCR. Expression was normalized to *EF-1α* transcript and set relative to Col-0. *n* = 8 biological replicates from 3 independent experiments. Centre line: median, bounds of box: 25th and 75th percentiles, whiskers: 1.5*IQR. No significant differences were identified between Col-0 and *pad4* (*P* > 0.05, two-sided Wilcoxon rank sum test with continuity correction). Exact *P* values are provided in Supplementary Table 5. **b**, Protein levels of FLS2, BAK1, MPK3, MPK4, and MPK6 are similar in Col-0 and *pad4* plants. Leaves were taken from three 6-week-old plants (labelled 1-3) and endogenous protein levels were evaluated by protein blot. Ponceau S-stained RUBISCO large subunit serves as a loading control. For gel source data, see Supplementary Fig. 1. The experiment was repeated at least three times with similar results.
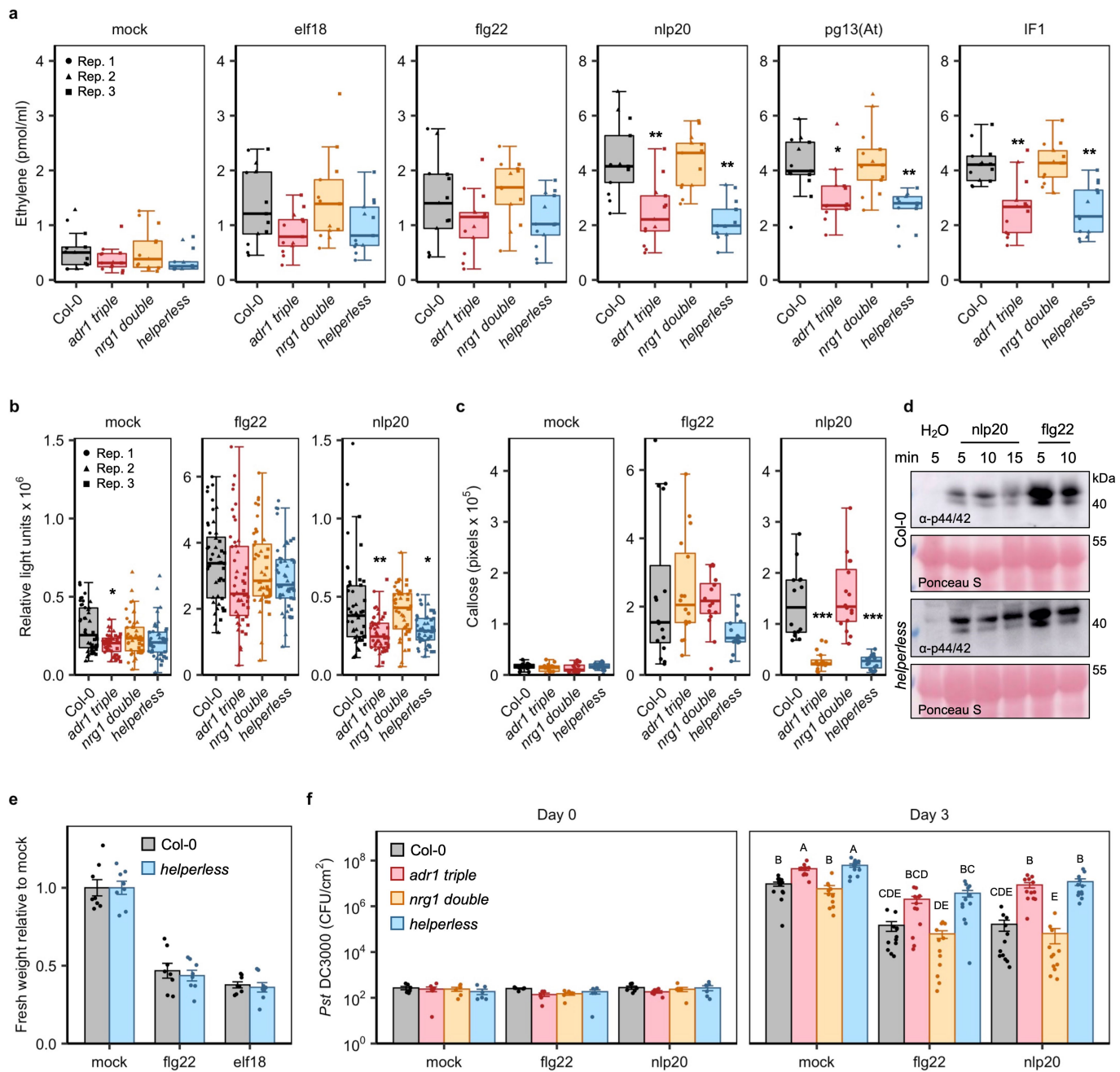
Extended Data Fig. 6 | ADR1 helper NLRs are positive regulators of LRR-RP signalling. a, Elicitor-induced ethylene production in helper NLR mutants. $n = 13$, each from 3 leaf pieces. Data are from 3 independent experiments. Col-0 is grey, *adr1 triple* is pink, *nrg1 double* is orange, and *helperless* is blue for all panels. For **a–c**, **f**, statistical differences between Col-0 and the indicated mutant for the given elicitor treatment were analysed using a Kruskal–Wallis test with post hoc two-sided Steel-Dwass test (*$P \le 0.05$, **$P \le 0.01$, ***$P \le 0.0001$). **b**, Total elicitor-induced ROS production over 30 min. $n = 48$ leaf discs from 3 independent experiments. **c**, Nlp20-induced callose deposition is reduced in *adr1 triple* and *helperless* mutants. $n \ge 12$ images from at least 3 leaves. For Col-0 nlp20, $n = 14$ images; for *adr1 triple* mock, $n = 15$; for all others $n = 16$. **d**, Representative immunoblot for MAP kinase activation in Col-0 and *helperless* treated with nlp20 or flg22. Ponceau S-stained RUBISCO large subunit serves as a loading control. For gel source data, see Supplementary Fig. 1. **e**, Relative fresh weight of 12 d-old Col-0 and *helperless* seedlings grown

in the presence of flg22 or elf18 ($n = 8$ biological replicates comprising 2 seedlings). No statistical differences between Col-0 and *helperless* were identified for each elicitor treatment ($P > 0.05$, two-sided student's *t*-test). **f**, Elicitor-induced defence against infection is impaired in *adr1 triple* and *helperless* mutants. Leaves were infiltrated with the indicated elicitor and challenged with *Pst* DC3000 24 h after infiltration. Bacterial colonization was assessed at Day 0 and Day 3. $n = 6$ (Day 0) or $n = 12$ (Day 3) biological replicates comprising 2 leaf discs. Bars with different letters indicate significant differences of $P \le 0.05$ (Kruskal–Wallis test with post hoc two-sided Steel-Dwass test). No statistical differences were observed for Day 0. CFU, colony forming units. For box plots in **a–c**, centre line: median, bounds of box: 25th and 75th percentiles, whiskers: 1.5 * IQR. For **e**, **f**, bars indicate mean ± s.e.m. Experiments in **c–f** were performed at least three times with similar results. Exact *P* values for all quantitative experiments are provided in Supplementary Table 5.
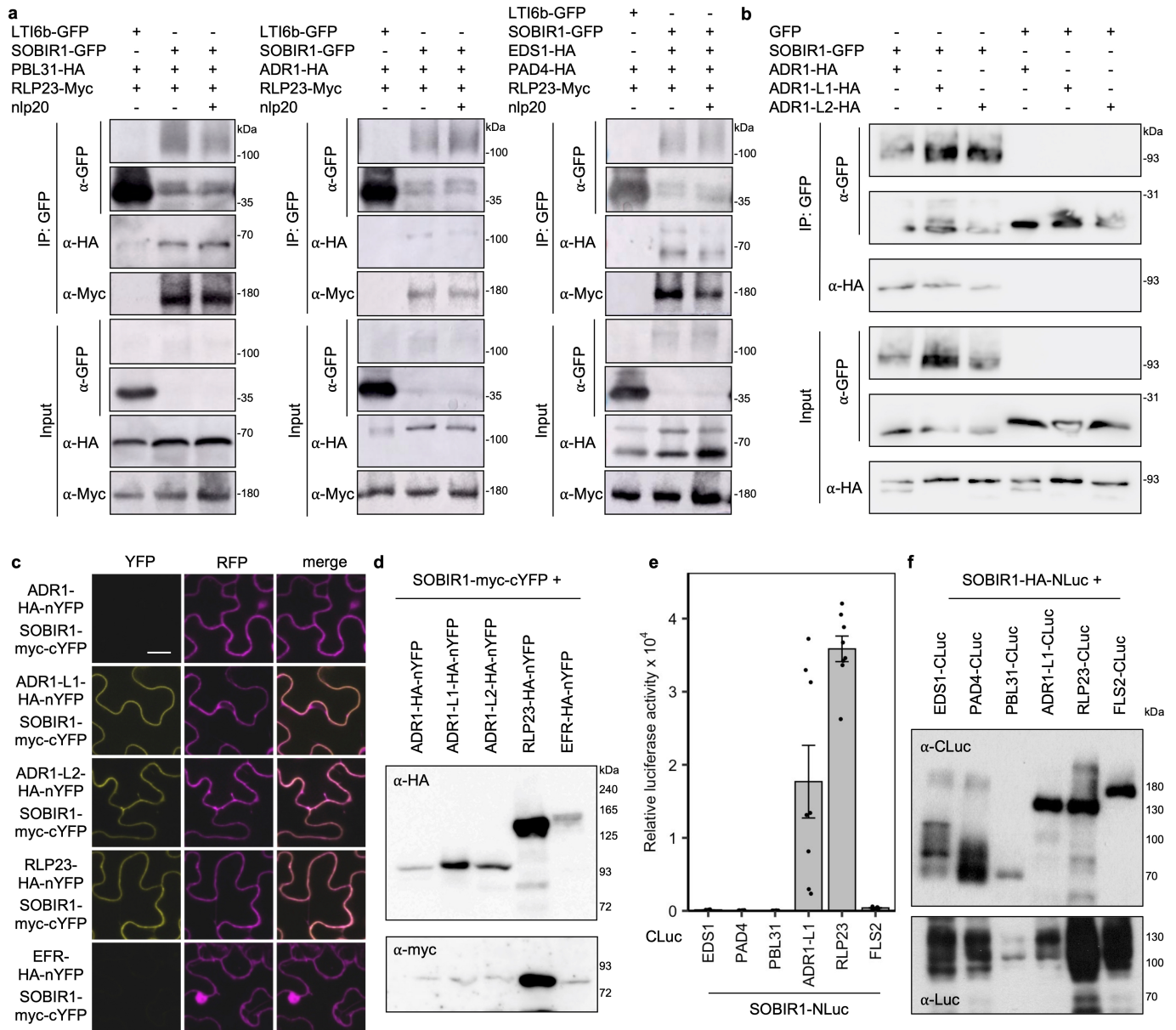
Extended Data Fig. 7 | Co-immunoprecipitation, split-YFP and split-luciferase complementation assays suggest that SOBIR1 is associated with multiple downstream signalling components. a, PBL31, ADR1, EDS1, and PAD4 associate with SOBIR1 in a nlp20-independent manner. The indicated proteins were transiently expressed in *Nicotiana benthamiana*. Leaves treated with nlp20 or water (mock) for 10 min were subjected to co-immunoprecipitation with GFP-trap beads. The proteins were not co-immunoprecipitated with a GFP-fused membrane protein (LTI6b[56]). The experiment was performed twice with similar results. **b**, Pull-down of GFP and SOBIR1-GFP transiently co-expressed with ADR1-HA, ADR1-L1-HA or ADR1-L2-HA. Plants transiently expressing the different proteins were subjected to co-immunoprecipitation using GFP-trap beads and subsequently analysed by protein blot using tag-specific antisera. ADR1-L1-HA and ADR1-L2-HA were co-immunoprecipitated at least three times with similar results; ADR1-HA was tested once. **c**, BiFC between SOBIR1 and the ADR1 isoforms confirms constitutive interaction of SOBIR1 with ADR1-L1 and ADR1-L2 at the plasma membrane. Scale bar indicates 20 μm. The experiment was performed at least three times with similar results. **d**, Protein levels of the transiently expressed proteins in BiFC experiments shown in panel **c**. **e**, Split luciferase complementation assays confirm the interaction of SOBIR1 and ADR1-L1. Bars indicate mean relative luciferase activity ± s.e.m.: *n* = 8 leaf discs from 4 leaves. The experiment was performed three times with similar results. **f**, Protein levels of the transiently expressed proteins in split luciferase experiments shown in panel **e**. Co-expression of the SOBIR1 and PBL31 constructs led to cell death and low protein abundance. The experiment was performed twice with similar results. For gel source data, see Supplementary Fig. 1.
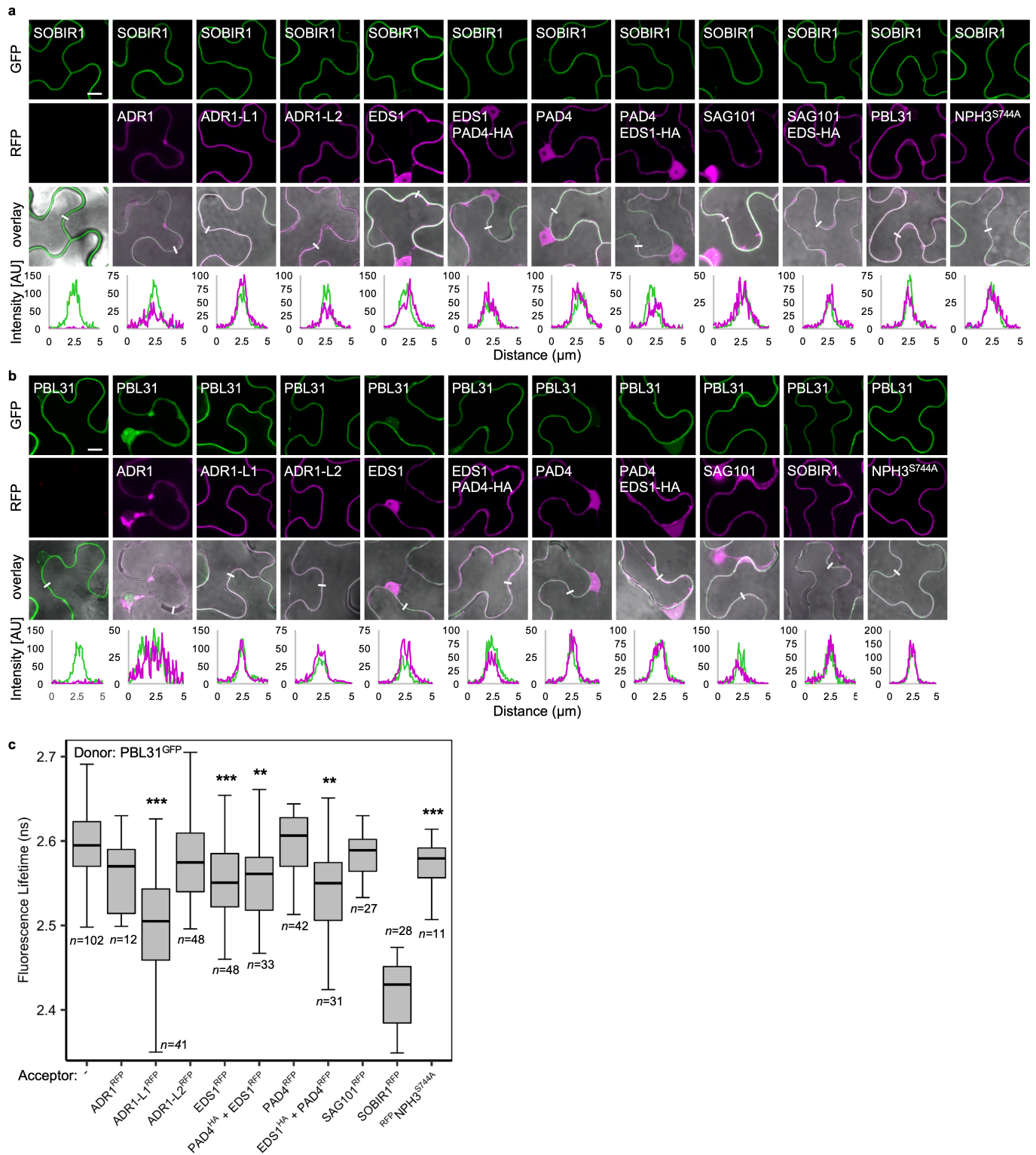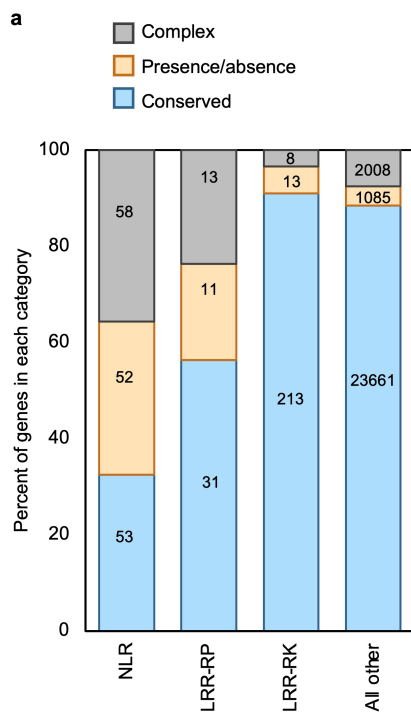
Extended Data Fig. 8 | FRET-FLIM analysis demonstrates association of PBL31-GFP with SOBIR1, ADR1-L1 and EDS1. a, b, Representative confocal images show co-localization of (**a**) SOBIR1-GFP or (**b**) PBL31-GFP with RFP fusions of ADR1, ADR1-L1, ADR1-L2, EDS1, PAD4, SAG101, (**a**) PBL31, or (**b**) SOBIR1 at the PM in transiently transformed *N. benthamiana* leaf cells. Plots show the GFP and RFP fluorescence intensity distribution across the PM in the indicated regions (white bars). Scale bars indicate 10 μm. This experiment was repeated three times with similar results. **c,** FRET-FLIM reveals spatial proximity of PBL31-GFP with ADR1-L1-RFP, EDS1-RFP, EDS1-RFP + PAD4-HA, PAD4-RFP + EDS1-HA and SOBIR1-RFP. Membrane-associated protein NPH3^{S744A} serves as control. $n \geq 11$ measurements from at least 3 biological replicates. Exact n values are shown below the boxes. Statistical differences in fluorescent lifetime from PBL31-GFP were analysed using a Kruskal–Wallis test with post hoc two-sided Steel-Dwass test (*$P \leq 0.05$, **$P \leq 0.01$, ***$P \leq 0.0001$). Exact P values are provided in Supplementary Table 5. Centre line: median, bounds of box: 25th and 75th percentiles, whiskers: 1.5*IQR.
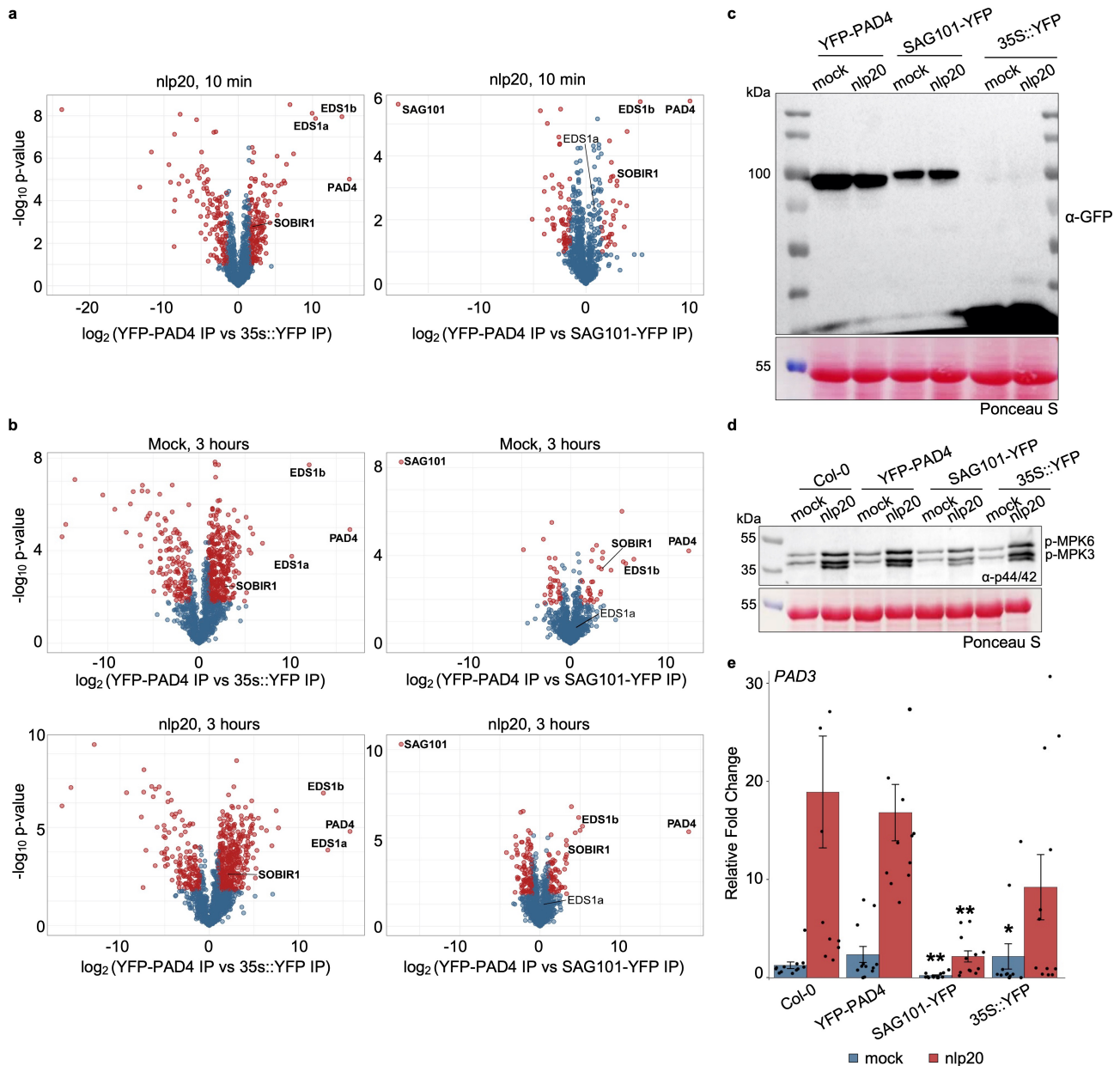
Extended Data Fig. 9 | SOBIR1 specifically co-purifies with YFP-PAD4 in Arabidopsis leaves in mock and nlp20-triggered conditions.
a, **b**, *Arabidopsis pad4-1/sag101-3* plants complemented with *pPAD4::YFP-gPAD4* (YFP-PAD4) or *pSAG101::gSAG101-YFP* (SAG101-YFP) or *35S::YFP* (YFP) in wild-type Col-0 background were used for immunoprecipitation (IP) assays. Volcano plots show normalized abundances (LFQ, log2 scale) of proteins detected in mass-spectrometry (MS) analyses after IP of total protein extracts from 4.5-week-old *Arabidopsis pad4-1/sag101-3* complementation lines or YFP control line infiltrated with **a**, nlp20 for 10 min, (**b**, upper panels) DMSO (Mock) for 3 h, and (**b**, lower panels) nlp20 for 3 h. Red dots indicate proteins enriched in YFP-PAD4 vs YFP samples (log2(YFP-PAD4 vs YFP) ≥ 1, left) and YFP-PAD4 vs SAG101-YFP samples (log2(YFP-PAD4 vs SAG101-YFP) ≥ 1, right), using permutation-based FDR = 0.05. Graphs represent significantly enriched peptides from four independent experiments (*n* = 4 per genotype per treatment). As shown for 10 min treatments (Fig. 3b), specific enrichment of the two functional Col-0 EDS1 isoforms (EDS1a and EDS1b) was detected in both YFP-PAD4 and SAG101-YFP samples, with EDS1b preferentially enriched following YFP-PAD4 pull-down. **c**, Representative immunoblot analyses to check test protein quality for IP quality in lines used for MS/MS analyses. Total protein extracts (IP inputs) from YFP-PAD4, SAG101-YFP and YFP lines

infiltrated with DMSO (mock) or nlp20 for 10 min. Inputs were subsequently immunoprecipitated using GFP-trap agarose beads and analysed by mass spectrometry. The analyses were repeated four times for both 10 min and 3 h treatments with similar results (*n* = 8 per genotype per treatment). **d**, **e**, Nlp20 treatment triggered immune responses at early (10 min) and late (3 h) time points in samples used for IP MS/MS analyses. **d**, Total protein extracts from Col-0, YFP-PAD4, SAG101-YFP and YFP lines infiltrated with DMSO (mock) and nlp20 for 10 min were analysed on immunoblots using an anti-p44/42-ERK antibody. The identity of individual phosphorylated (p)-MAPKs, as determined by their mobility, is indicated by arrows. The analysis was repeated four times with similar results (*n* = 4 samples per genotype per treatment). For gel source data, see Supplementary Fig. 1. **e**, *PAD3* transcript levels were determined by qRT–PCR at 3 h after mock (DMSO) or nlp20 treatment of the indicated genotypes. Relative expression was normalized to *UBQ5* and set to Col-0 mock samples. Bars indicate mean expression ± s.e.m. (*n* = 12 biological replicates from 4 independent experiments). Statistical differences between Col-0 and the indicated genotypes were analysed using Kruskal–Wallis with post hoc two-sided pairwise comparisons using Wilcoxon rank sum test with a Benjamini-Hochberg correction (*$P \leq 0.05$, **$P \leq 0.01$). Exact P values are provided in Supplementary Table 5.

a

Legend:
- ☐ Complex (grey)
- ☐ Presence/absence (orange)
- ☐ Conserved (blue)

Y-axis: Percent of genes in each category (0–100)

X-axis categories: NLR, LRR-RP, LRR-RK, All other

Bar values:
- NLR: Complex 58, Presence/absence 52, Conserved 53
- LRR-RP: Complex 13, Presence/absence 11, Conserved 31
- LRR-RK: Complex 8, Presence/absence 13, Conserved 213
- All other: Complex 2008, Presence/absence 1085, Conserved 23661

b

COMPLEX

RLP5 (AT1G34290)	RLP38 (AT3G23120)	RLP43 (AT3G28890)
RLP7 (AT1G47890)	RLP39 (AT3G24900)	RLP47 (AT4G13810)
RLP13 (AT1G74170)	RLP40 (AT3G24982)	RLP56 (AT5G49290)
RLP34 (AT3G11010)	RLP41 (AT3G25010)	
RLP37 (AT3G23110)	**RLP42 (AT3G25020)**	

PRESENCE/ABSENCE

RLP1 (AT1G07390)	RLP16 (AT1G74200)	RLP36 (AT3G23010)
RLP2 (AT1G17240)	RLP24 (AT2G33020)	RLP48 (AT4G13880)
RLP3 (AT1G17250)	RLP25 (AT2G33030)	RLP50 (AT4G13920)
RLP11 (AT1G71390)	RLP28 (AT2G33080)	

CONSERVED

RLP4 (AT1G28340)	RLP21 (AT2G25470)	RLP44 (AT3G49750)
RLP6 (AT1G45616)	RLP22 (AT2G32660)	RLP45 (AT3G53240)
RLP8 (AT1G54470)	**RLP23 (AT2G32680)**	RLP46 (AT4G04220)
RLP9 (AT1G58190)	RLP26 (AT2G33050)	RLP51 (AT4G18760)
RLP10 (AT1G65380)	RLP27 (AT2G33060)	RLP52 (AT5G25910)
RLP12 (AT1G71400)	RLP29 (AT2G42800)	RLP53 (AT5G27060)
RLP14 (AT1G74180)	**RLP30 (AT3G05360)**	RLP54 (AT5G40170)
RLP15 (AT1G74190)	RLP31 (AT3G05370)	RLP55 (AT5G45770)
RLP17 (AT1G80080)	**RLP32 (AT3G05650)**	RLP57 (AT5G65830)
RLP19 (AT2G15080)	RLP33 (AT3G05660)	
RLP20 (AT2G25440)	RLP35 (AT3G11080)	

Extended Data Fig. 10 | Classification of LRR-RPs, LRR-RKs and NLRs according to genetic conservation in *Arabidopsis* accessions. a, Reads from 80 *Arabidopsis* accessions were mapped to the reference genome of Col-0. Genes were categorised as being conserved, having complex patterns of variation or exhibiting presence/absence polymorphisms according to the distribution of large-scale polymorphisms across all accessions as inferred from stringent read mappings. Criteria for categorization are detailed in the Methods. The numbers of genes falling into each category are provided in the corresponding bars. **b**, LRR-RP genes classified as in **a**. Genes encoding known immune receptors are indicated in bold.